GLOBAL BIOGEOCHEMICAL CYCLES, VOL. 13, NO 2, PAGES 287-305, JUNE 1999

Spatial distribution of air-sea CO_2 fluxes and the interhemispheric transport of carbon by the oceans

R. J. Murnane

Risk Prediction Initiative, Bermuda Biological Station for Research, St. George's, Bermuda

J. L. Sarmiento

Program in Atmospheric and Oceanic Sciences, Department of Geosciences, Princeton University, Princeton, New Jersey

C. Le Quéré

Laboratoire des Sciences du Climat et de l'Environnement, Gif-sur-Yvette, France

Abstract. The dominant processes controlling the magnitude and spatial distribution of the preindustrial air-sea flux of CO_2 are atmosphere-ocean heat exchange and the biological pump, coupled with the direct influence of ocean circulation resulting from the slow time-scale of air-sea CO_2 gas exchange equilibration. The influence of the biological pump is greatest in surface outcrops of deep water, where the excess deep ocean carbon resulting from net remineralization can escape to the atmosphere. In a steady state other regions compensate for this loss by taking up CO_2 to give a global net air-sea CO_2 flux of zero. The predominant outcrop region is the Southern Ocean, where the loss to the atmosphere of biological pump CO_2 is large enough to cancel the gain of CO_2 due to cooling. The influence of the biological pump on uptake of anthropogenic CO_2 is small: a model including biology takes up 4.9% less than a model without it. Our model does not predict the large southward interhemispheric transport of CO_2 that has been suggested by atmospheric carbon transport constraints.

1. Introduction

A number of recent papers have challenged our understanding of the ocean carbon cycle and its role in the global carbon cycle [*Maier-Reimer and Hasslemann*, 1987; *Bacastow and Maier-Reimer*, 1991; *Quay et al.*, 1992; *Francey et al.*, 1995; *Keeling et al.*, 1995; *Bacastow et al.*, 1996; *Heimann and Maier-Reimer*, 1996; *Yamanaka and Tajika*, 1996, 1997; *Joos and Bruno*, 1998]. The analysis of global air-sea ΔpCO_2 observations reported by *Tans et al.* [1990] gives a substantial oceanic uptake of CO_2 concentrated primarily in the Southern Hemisphere. However, Tans et al. found from an atmospheric model constrained by pCO_2 observations that southward atmospheric transport from the big Northern Hemisphere fossil fuel sources was too small to support a large oceanic uptake of CO_2 in the Southern Hemisphere. Their observationally based estimate of carbon uptake by the Northern Hemisphere ocean gives only 0.6 Pg C yr^{-1}. When put together with other components of the global carbon budget, this led Tans et al. to propose a total oceanic anthropogenic carbon uptake of only 0.3-0.8 Pg C yr^{-1}, less than half the 2.0 ± 0.6 Pg C yr^{-1} estimate based on radiocarbon calibrated ocean models [cf. *Orr* ,[1993]; *Siegenthaler and Sarmiento*, 1993; *Schimel et al.*, 1995].

Paper number 1998GB900009.
0886-6236/99/1998GB900009$12.00

Part of the discrepancy between the *Tans et al.* [1990] estimate and the radiocarbon estimates can be reconciled if one considers the ~0.4-0.7 Pg C yr^{-1} difference in flux estimates due to the combined influence of the thermal skin effect, the return of CO_2 to the atmosphere due to the oxidation of organic carbon brought to the ocean from rivers, and the precipitation of carbonate to close the silicate and carbonate weathering cycle [*Sarmiento and Sundquist*, 1992].

Keeling et al. [1989] came to the same conclusion as *Tans et al.* [1990] regarding the finding that southward atmospheric transport of CO_2 was too small to support a large carbon uptake by the Southern Ocean. However, *Keeling et al.* [1989] kept the large oceanic sink (2.3 Pg C yr^{-1} in their study) and proposed instead that the Northern Hemisphere oceanic uptake must be extremely large. Given that most of the ocean's surface area is in the Southern Hemisphere and that therefore most of the oceanic uptake of anthropogenic carbon must be there [cf. *Sarmiento et al.* 1992], this proposal implies that there must have been a large preindustrial loss of carbon to the atmosphere in the Southern Hemisphere balanced by uptake in the Northern Hemisphere. The anthropogenic perturbation of the atmosphere would reduce the Southern Hemisphere CO_2 source and increase the Northern Hemisphere CO_2 oceanic sink thus giving the desired present pattern of a small Southern Hemisphere ocean flux and large Northern Hemisphere uptake. The preindustrial air-sea fluxes [*Keeling et al.*, 1989] would have been balanced by a northward transport of carbon within the atmosphere and a southward transport within the ocean. *Keeling et al.* [1989] showed that the time

Table 1. Air-Sea CO_2 Fluxes

	1990	1972-1988	1981-1987	1984	1990	Preindustrial	
	Present study[a]	[*Tans et al.*, 1990][b]	[*Tans et al.*, 1990][c]	[*Keeling et al.* 1989]	[*Takahashi et al.*, 1997][d]	Present Study[e]	[*Keeling et al.* 1989][f]
15°N-90°N	1.2	0.6	0.3 - 0.6	2.3	0.9	0.6	1.7
15°S-15°N	-0.7	-1.6	-1.3 - -0.7	-1.1	-0.7	-1.2	-1.8
90°S-15°S	1.8	2.6	0.6 - 1.4	1.1	1.0	0.6	0.1
Total	2.3	1.6	0.3 - 0.8	2.3	1.1	0.0	0.0

Fluxes given in Pg C yr^{-1}

a) Fluxes based on 1990 results from the OBM.

b) Annual air-sea fluxes based on measurements over the 1981 to 1988 period. These fluxes ignore the constraints provided by the atmospheric transport model and observations.

c) Annual air-sea fluxes based on model scenarios that adjust ocean fluxes in an atmospheric transport model to minimize the differences between predicted and measured atmospheric pCO_2 over the 1981 to 1987 period.

d) Based on compilation of ΔpCO_2 data .

e) Steady state preindustrial air-sea carbon fluxes from the OBM.

f) Based on the equatorial and North Atlantic fluxes for 1984.

history of the South Pole to Mauna Loa atmospheric pCO_2 difference is consistent with the atmospheric branch of this cycle, and *Broecker and Peng* [1992] confirmed from an analysis of observations that the oceanic branch of the cycle might also exist within the Atlantic Ocean [see also *Keeling and Peng*, 1995].

The *Keeling et al.* [1989] and *Tans et al.* [1990] studies suggest that although the total oceanic uptake of anthropogenic carbon for 1980-1989 (2.0± 0.6 Pg C yr^{-1} [*Schimel et al.*, 1995]) is known fairly well, our understanding of the spatial distribution of air-sea CO_2 fluxes is very poor. The total ocean uptake estimate includes within its range the recent challenge to previous budgets by *Hesshaimer et al.* [1994] based on their reanalysis of the global radiocarbon budget, which itself has been challenged by *Broecker and Peng* [1994] and *Joos* [1994]. As illustrated by the preindustrial air-sea flux summary in Table 1, the final conclusion of the analysis by *Keeling et al.* [1989] is that the large equatorial degassing is balanced primarily by a Northern Hemisphere uptake, whereas the data analysis of ΔpCO_2 presented by *Tans et al.* [1990] suggests that equatorial degassing is balanced primarily by Southern Hemisphere uptake. The ocean general circulation model results we present here have a smaller equatorial efflux balanced by approximately equal uptake fluxes in both hemispheres.

The major aim of this study is to use an ocean biogeochemistry model (OBM) to provide an independent constraint on the oceanic source-sink CO_2 distribution and to improve our understanding of the processes that control that distribution. Partial results of the Princeton OBM have been previously described by *Sarmiento et al.* [1995] in a paper on the North Atlantic that also includes a comparison with observations. The Hamburg Max Planck Institute ocean carbon cycle model [*Maier-Reimer and Hasslemann*, 1987; *Bacastow and Maier-Reimer*, 1990; *Kurz and Maier-Reimer*, 1993; *Maier-Reimer*, 1993] includes many of the same elements as our model, though our approach to doing the biological pump is different.

Our analysis of the OBM separates the carbon cycle into two components that are due to the solubility and biological pumps. *Volk and Hoffert* [1985] introduced the pump concept to describe the oceanographic processes that create and maintain concentration gradients in the ocean. The solubility pump arises from the interaction of ocean circulation with the heat and water cycles. Surface fluxes of heat and water change the solubility of CO_2 and speciation of carbon and lead to locally large air-sea fluxes (up to 6.42 mol C m^{-2} yr out of the ocean and 10.30 mol m^{-2} yr^{-1} into the ocean) that must be balanced by ocean transport. On a global scale the impact of the solubility pump is to give higher deep ocean concentrations because of the fact that the cold waters that fill the abyss have a higher carbon-holding capacity than warmer surface waters. The global air-sea flux due to the solubility pump is zero in a steady state. However, locally the fluxes can be quite large, creating features such as the significant loss of CO_2 from equatorial region due to warming of relatively cold upwelled water. This CO_2 loss is offset by the gain of CO_2 in high latitudes due to cooling.

We define the biological carbon pump as the formation of dissolved and particulate organic carbon and $CaCO_3$ and the transport of these materials to other regions of the ocean where they are dissolved or remineralized. This is primarily a vertical flux that removes inorganic carbon from the surface ocean and releases it at depth thus increasing the vertical carbon gradient substantially above that which would be obtained with the solubility pump alone. Ocean circulation transports inorganic carbon from the abyss back to the surface. In a steady state and on a global scale the loop involving the biological pump must be closed within the ocean, that is, the upward transport of inorganic carbon must balance exactly the downward biological pump flux, and the net air-sea flux must be zero. There are small sinks of carbon in ocean sediments due to river inputs and burial of organic carbon and $CaCO_3$, but these are ignored in the present version of the model (see *Sarmiento and Sundquist* [1992] for a review of the role of these processes in the global carbon budget). The high abyssal carbon concentrations resulting from the biological pump outcrop at the surface in a number of locations. Here there will be an outgassing flux to the atmosphere that must be balanced by a compensatory uptake elsewhere in low carbon regions. As with the solubility pump, the local air-sea fluxes resulting from the biological pump can be quite large.

An ideal way to study the relative roles of the solubility and biological pumps would be to run separate simulations of each of these. If carbon chemistry were linear, then the sum of these two

simulations would give the same result as running the two pumps simultaneously. However, carbon chemistry is not linear. Our approach is thus to carry out parallel simulations of our OBM and an abiotic solubility model, fixing atmospheric pCO_2 at the same preindustrial value of 278.2 μatm in both cases. We take the difference between these two models as representing the incremental contribution of the biological pump. The contribution of the solubility and biological pumps to local air-sea fluxes has been explored previously for some regions of the ocean by *Volk and Liu* [1988] using limited area models. Our study uses a global model thus removing the ambiguities in the Volk and Liu study that arise from not being able to close the carbon budget with a local area model.

In addition to the pumps, limited rates of air-sea gas exchange also affect air-sea CO_2 fluxes and distributions in the ocean. We estimate the effects of gas exchange on CO_2 fluxes and dissolved inorganic carbon distributions by comparing OBM and solubility model results to "potential OBM" and "potential solubility model" results. In the potential models, surface ocean CO_2 is restored to equilibrium with the atmosphere at each time step using a constant gas transfer velocity. The gas transfer velocity in the potential model runs is $\Delta z/\Delta t$ = 42 m d^{-1}, where Δz is the surface layer thickness (50 m) and Δt is the model time step. With this gas transfer velocity the timescale for ventilating the surface layer with a simple gas is equal to the model time step of ~1 day. For comparison, the global mean of the area-weighted gas transfer velocity in the OBM and solubility model is 4.3 m d^{-1}.

An additional aim of our study is to clarify the relative roles of the solubility and biological pumps in the direct uptake of anthropogenic carbon from the atmosphere. This subject has been the source of considerable controversy and misunderstanding (e.g., see *Broecker* [1991] and replies by *Banse* [1991], *Sarmiento* [1991], and *Longhurst* [1991]). The simulations described here enable us to make a specific quantitative (albeit model based) assessment of the role that the biological pump plays in oceanic uptake of anthropogenic carbon.

2. Model Description

We use an annual mean 4° version of the Geophysical Fluid Dynamics Laboratory primitive equation modular ocean model (MOM) code [*Pacanowski et al.*, 1993]. A description of the original circulation model, its ability to reproduce the observed uptake of ^{14}C, small modifications to the model, and the impact of these changes on tracer transport are described elsewhere [*Toggweiler et al.*, 1989; *Toggweiler and Samuels*, 1993a, 1993b]. The total model depth of 5000 m is represented by 12 levels of increasing thickness. The thickness of the top, second, and bottom levels is 50.9 m, 68.4 m, and 869 m, respectively.

Among the biologically utilized tracers carried in the model are phosphate, oxygen, dissolved inorganic carbon (DIC), total alkalinity (TA), and labile dissolved organic carbon (LDOC). Later in the text we use the term "passive tracer" to characterize biologically utilized tracers. The term passive tracer refers to the fact that they have no effect on ocean circulation. New production in the model is based on a phosphate restoring technique [*Najjar et al.*, 1992], and stoichiometric ratios ($P:C:-O_2$ = 1:120:170) are used to convert biologically related phosphate fluxes to carbon and oxygen fluxes. As a first order approximation, new production is split evenly between particulate organic carbon (POC) and LDOC formation. Export and remineralization of particulate material is modeled implicitly using a power law relationship [*Martin et al.*, 1987]. Carbonate cycling is based on an approach that restores global level mean alkalinity in the model to an idealized alkalinity profile based on a volume-weighted average of Geochemical Ocean Sections Studty (GEOSECS) data. A global level mean carbonate to POC ratio is used to predict local carbonate precipitation and dissolution from local POC production and remineralization. We do not differentiate between the Southern Ocean and the remainder of the basins in apportioning the $CaCO_3$ production.

The LDOC represents the dissolved organic carbon (DOC) fraction that produces the upper ocean increase in DOC concentration above the deep water background. The mean ocean concentration of LDOC (4.2 μM) is conserved in the model by equating global ocean LDOC remineralization and production. Remineralization of LDOC is based on a first-order decay constant that has a value of 1/11.2 yr^{-1} after equilibration of the model. The remineralization rate constant for our LDOC is much slower than the 1/0.5 yr^{-1} rate constant for semilabel DOC modeled by *Yamanaka and Tajika* [1997]; however, Yamanaka and Tajika include a refractory phase in their model and assume that the semilabel dissolved organic matter/particulate organic matter (DOM/POM) production ratio is 2. Increasing the DOM/POM production ratio in our model by a factor of 4 (from 0.5 to 2) would greatly increase the LDOC remineralization rate.

An additional "virtual" flux of tracers at the surface is added to account for dilution and concentration of passive tracers due to implicit water fluxes in the ocean model. The rigid lid approximation used in the ocean model does not permit air-sea water fluxes, so virtual fluxes are calculated from salt fluxes produced by salinity-restoring terms in the salt conservation equation. Further details of the model are given in the appendix.

Our model does not include seasonal variability. Adding seasonality to the model requires a different treatment of biological processes than the observationally based forcing that we use here (see, for example, *Maier-Reimer and Hasslemann* [1987]; *Bacastow and Maier-Reimer* [1990]; *Maier-Reimer and Bacastow* [1990]; *Kurz and Maier-Reimer* [1993]; and *Maier-Reimer* [1993] who use simple predictive models). Clearly, this is an important omission from the model. We are working to redress it at present [cf., *Sarmiento et al.* [1993]; *Fasham et al.* [1993]. However, from past experience with simulations of temperature and salinity as well as tracer distributions, we do not expect the impact of seasonality to be great on the large scales that we address here. Because of the relatively slow timescales of ocean circulation, the direct impact of seasonal processes on ocean carbon distributions is generally localized [cf. *Follows et al.*, 1996]. The same is not true of interannual variability, which, however, we do not address as part of this study. For an interesting recent carbon modeling study of the impact of interannual variability due to El Niño, see *Winguth et al.* [1994].

We produce an ocean in equilibrium with the preindustrial atmosphere by fixing atmospheric pCO_2 at 278.2 μatm (dry atmosphere value) and allowing CO_2 to invade the ocean until the globally integrated air-sea flux of CO_2 is negligible. We then use this model as an initial condition for simulations of the time history of the anthropogenic transient. Simulations of the oceanic uptake of anthropogenic carbon are performed by fixing the atmospheric CO_2 content at its observed concentration time history and allowing it to invade the ocean. The anthropogenic carbon component in the ocean model is defined as the difference be-

tween the flux or concentration in the ocean at a given time and the steady state preindustrial value. The CO_2 concentration history is determined from trapped air bubbles in South Pole and Siple ice cores [*Neftel et al.*, 1985; *Friedli et al.*, 1986] and measurements made at Mauna Loa [*Keeling and Whorf*, 1991] [cf. *Sarmiento et al.*, 1992 and *Siegenthaler and Joos*, 1992].

3. Solubility Model

We run our carbon model simulations until the DIC content achieves a steady state and the globally integrated sea-air flux is zero. As a consequence of the steady state requirement, the loss of carbon from the ocean to the atmosphere in one region must be balanced by a net transport of carbon within the ocean from regions of gain from the atmosphere. The main emphasis of sections 3-5 is on the mechanisms that give rise to the sea-air fluxes in the solubility and biological pumps and the processes by which carbon is transferred within the ocean from regions of carbon gain to regions of carbon loss.

Air-sea fluxes of CO_2 in the potential solubility and solubility models are due mainly to heating and cooling of surface waters and the resultant change in CO_2 solubility. Cooling of surface waters in high latitudes increases gas solubility and results in oceanic uptake of CO_2; warming of surface waters in low latitudes decreases gas solubility and results in the release of oceanic CO_2. Other factors that affect gas fluxes are water (salt) fluxes, which alter gas solubility, ocean circulation, and gas exchange kinetics.

Air-sea CO_2 fluxes in the potential solubility model are the result of the combined effects of heat and water fluxes at the surface ocean. The thermal flux of a gas is predicted from temperature dependent changes in gas solubility due to air-sea heat fluxes. The thermal flux of CO_2 [cf. *Keeling et al.*, 1993] can be estimated using heat fluxes and the buffer factor R to account for the nonlinear dependence of $[CO_2]$ on DIC:

$$F_{CO_2} = \frac{Q}{\rho C_p}\frac{\partial [DIC]_{eq}}{\partial T} = \frac{Q}{\rho C_p}\frac{\partial [CO_2]_{eq}}{\partial T}\frac{1}{R}\frac{[DIC]}{[CO_2]} \qquad (1)$$

where C_p is the heat capacity of seawater (cal deg^{-1} g^{-1}), ρ is density (g cm^{-3}), Q is the modeled heat flux (cal cm^{-2} s^{-1}), T is sea surface temperature (degrees), and $[CO_2]_{eq}$ is the equilibrium CO_2 concentration for a given temperature, salinity, and pCO_2 (mol cm^{-3}). The buffer factor is the fractional change in CO_2 divided by the fractional change in DIC after equilibrium

$$R = \frac{\partial [CO_2]/[CO_2]}{\partial [DIC]/[DIC]}$$

The zonal mean thermal flux of CO_2 is very close to the potential flux of CO_2 in the potential solubility model because heat fluxes are the dominant factor affecting changes in DIC solubility (Figure 1). Water fluxes have a very small effect on air-sea CO_2 fluxes.

The solubility model CO_2 fluxes differ dramatically from the potential fluxes because of the long timescale (mean time of 7 months) for DIC equilibration of the surface model layer (51.9 m) with the atmosphere. The long equilibration time can be understood by considering mass balance equations for DIC and CO_2 in a box equilibrating with an atmosphere with constant pCO_2 [*Najjar*, 1992]. The concentration of DIC in the box will change only because of gas exchange:

$$\frac{\partial [DIC]}{\partial t} = \frac{k_g}{\Delta z}([CO_2]_{atm} - [CO_2]) \qquad (2)$$

where k_g is the gas transfer velocity, $[CO_2]_{atm}$ is the CO_2 concen-

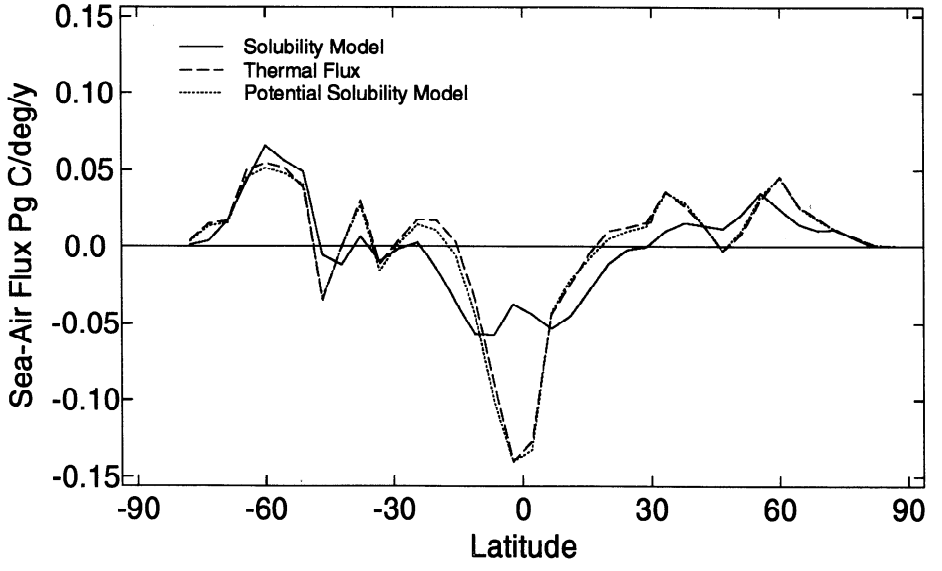

Figure 1. Solubility model CO_2 air-sea flux, the thermal flux predicted using equation (2), and the potential solubility model CO_2 flux. Positive fluxes are into the ocean. The overall structure shows release of CO_2 in low latitudes due to heating of surface waters and the decrease in dissolved inorganic carbon (DIC) solubility and absorption of CO_2 in high latitudes due to cooling of surface waters and an increase in DIC solubility. Solubility model fluxes near the equator are spread over a wide latitude range because of the 7 month air-sea equilibration time for DIC in the surface layer.

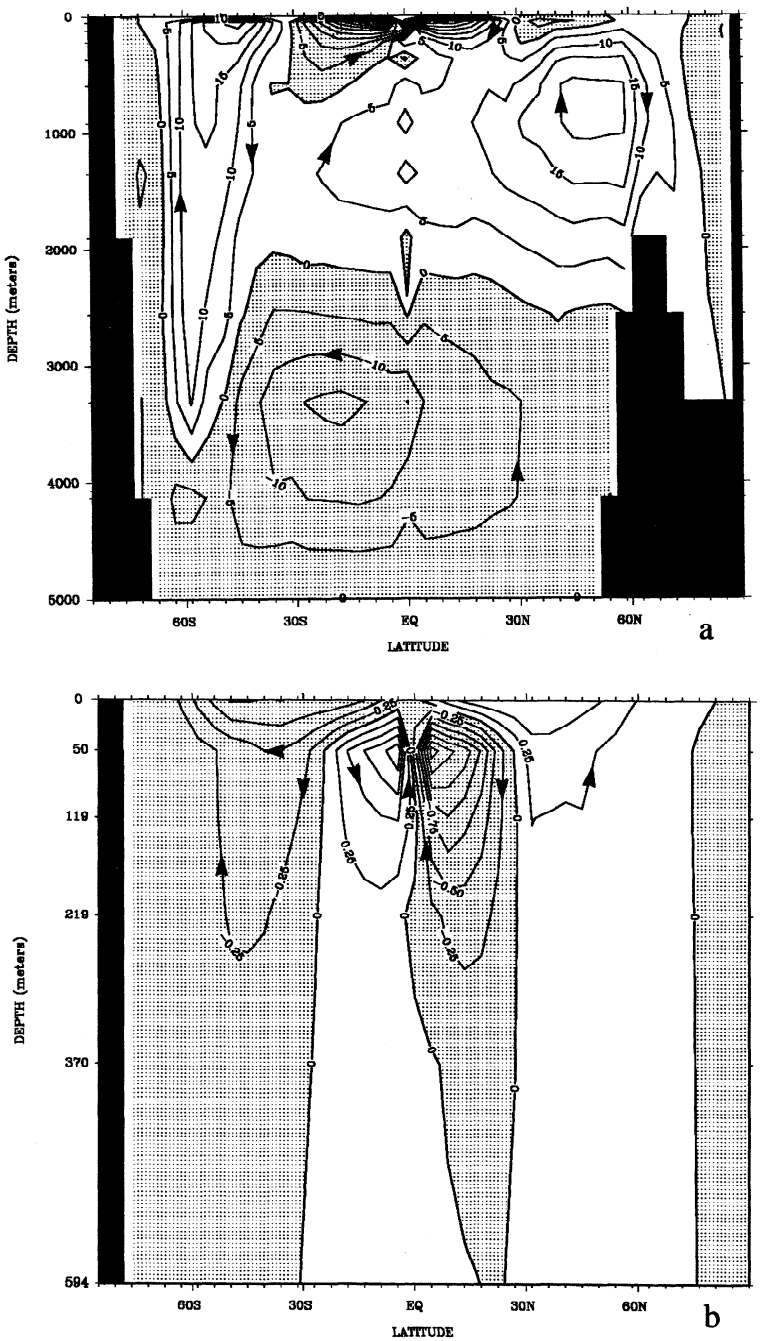

Figure 2. (a) Ocean meridional overturning in sverdrups (10^6 m^3 s^{-1}). (b) Meridional transport of perturbation carbon obtained by subtracting the ocean mean DIC content.

tration in equilibrium with the atmosphere, and $[CO_2]$ is the surface layer CO_2 concentration. Most of the CO_2 that enters the ocean will react with dissolved carbonate ions, so there is not a linear relationship between $[DIC]$ and $[CO_2]$. The buffer factor relationship can be used to substitute for $[DIC]$ in the left-hand side of (2). The mass balance equation for $[CO_2]$ is thus

$$\frac{\partial[CO_2]}{\partial t} = \frac{k_g R[CO_2]}{\Delta z[DIC]}([CO_2]_{atm} - [CO_2]) \quad (3)$$

The mass balance equation for a gas that does not chemically react with water lacks the term $R[CO_2]/[DIC]$, which is of the order of 1/20 in our model. Thus $[CO_2]$ changes at about 1/20th the rate of a gas such as oxygen. The mismatch between potential and wind speed dependent CO_2 fluxes can thus be quite large in regions such as the equator, where horizontal Ekman transport displaces water poleward on short timescales relative to air-sea CO_2 equilibration time scales. In other regions, water is subducted before equilibration can occur.

Any net flux of CO_2 across the sea-air interface must be balanced by transport within the ocean. On a large scale most of the oceanic transport is by advection. Figure 2a shows the merid-

ional overturning predicted by the ocean circulation model. The DIC content of the ocean averages 2085 μmol kg^{-1} in the solubility model, but the global range in DIC is only 8.4% of the total DIC. Thus most of the carbon transport resulting from the meridional overturning will be in closed loops, like the transport of water itself, with each sverdrup (10^6 m^3 s^{-1}) of water transporting 0.8 Pg C yr^{-1}. Subtracting the mean DIC concentration before calculating the ocean transport gives the perturbation to the transport associated with the air-sea and virtual fluxes of carbon. Most of the perturbation transport is quite shallow (Figure 2b). The loss of CO_2 at the equator is balanced primarily by gain in the equatorward half of the subtropical gyres and transport through the upper thermocline. The amount of carbon supplied by transport from below 300-400 m is negligible.

On a global scale there is essentially no interhemispheric transport of DIC in the potential solubility model (Figure 3a) because there is essentially no interhemispheric transport of heat by the model ocean. Decoupling of heat and CO_2 air-sea fluxes by the wind speed dependent gas exchange of the solubility model could result in global interhemispheric transport of carbon. However, the solubility model predicts only a small amount of global interhemispheric transport because most transport of carbon occurs within overturning cells that involve Ekman transport at the surface and that close within a hemisphere (Figure 2). Interhemispheric transport of carbon in the solubility model would require some mechanism for significant interhemispheric transport of heat or a mechanism that could transport significant amounts of DIC between hemispheres independent of heat.

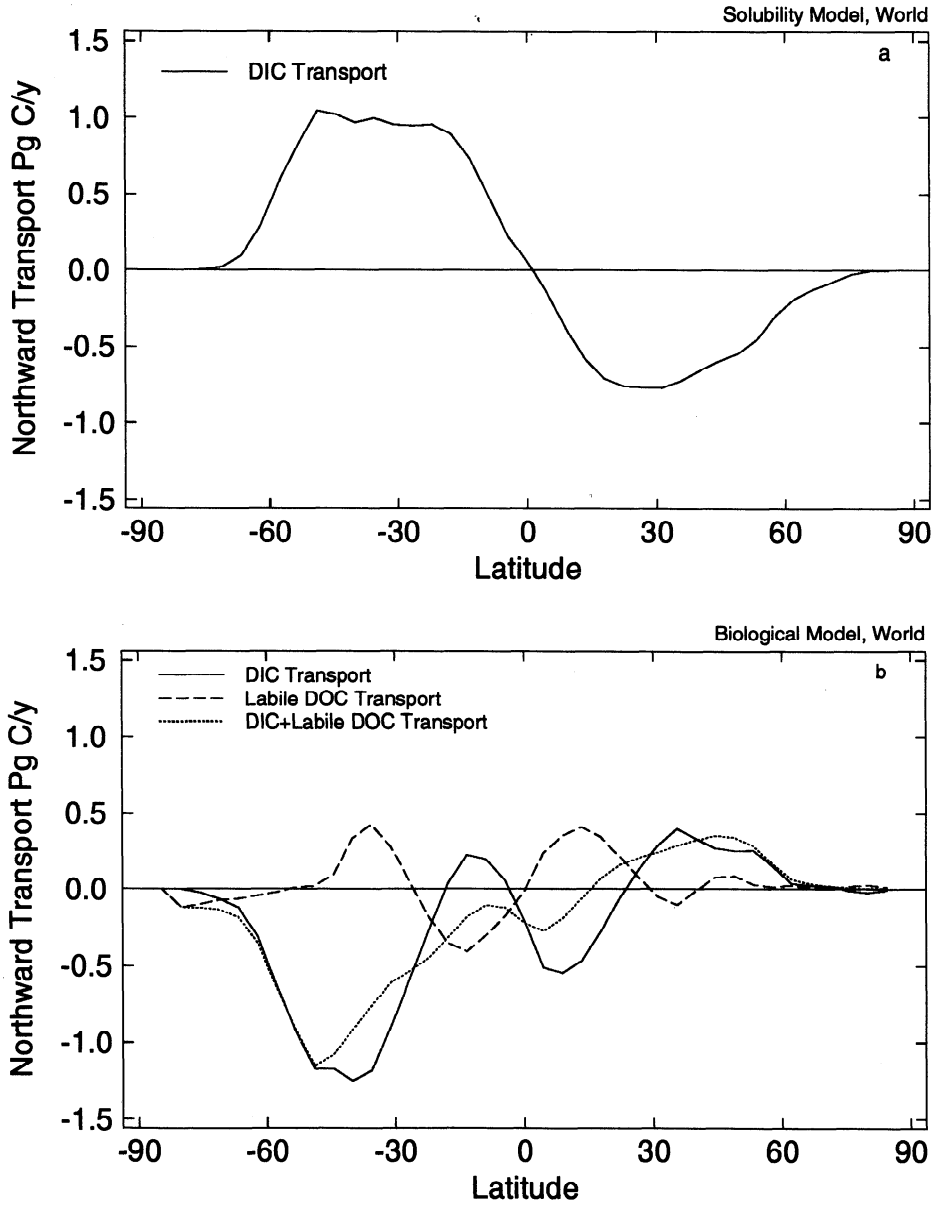

Figure 3. (a) Northward transport of DIC by the solubility model. (b) Biological model northward transport of DIC, labile dissolved organic carbon (DOC), and DIC plus labile DOC transport. (c) Ocean biogeochemistry model (OBM) northward transport of DIC, labile DOC, and DIC plus labile DOC transport.

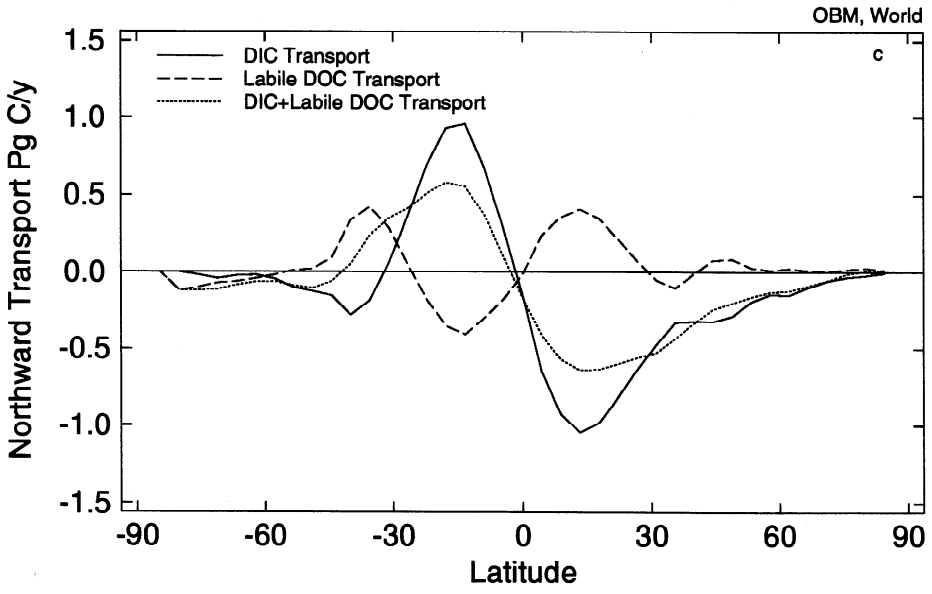

Figure 3. (continued)

The global carbon inventory predicted with the solubility model is 37,409 Pg C (1 Pg=1 Gt=10^{15}g). The vast majority of this carbon is in the form of bicarbonate and carbonate ion. Only 250 Pg C would dissolve in the ocean if CO_2 did not react with water and dissociate to form these ions. The mean DIC concentration is 2085 μmol kg^{-1}, much lower than the observed global mean concentration of 2268 μmol kg^{-1} obtained from GEOSECS observations (Figure 4). The reason the solubility model carbon inventory is lower than the observations is because the model lacks the biological processes that increase the deep ocean concentration. The global mean concentration in the solubility model is only 65 μmol kg^{-1} higher than the surface mean concentration of 2020 μmol kg^{-1}. By contrast, the observed global mean concentration of 2268 μmol kg^{-1} is 240 μmol kg^{-1} greater than the observed surface mean concentration of 2028 μmol kg^{-1}.

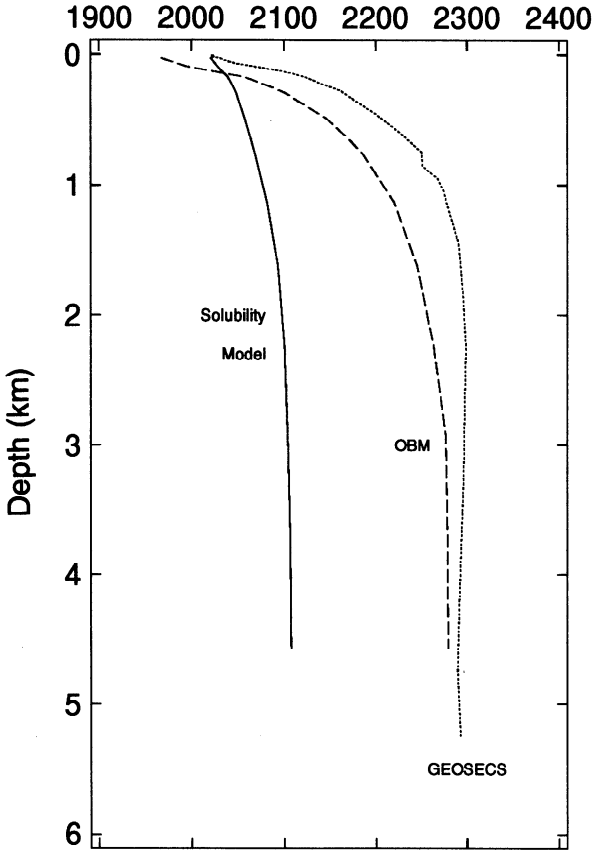

Figure 4. Global average DIC (μmol kg^{-1}) profiles for the preindustrial solubility model and OBM and for an average of Global Ocean Sections Study (GEOSECS) analyses.

4. Ocean Biogeochemistry Model

Organic carbon export from the surface by the biological pump is 6.88 Pg C yr^{-1} of particulate organic matter and 4.22 Pg C yr^{-1} of dissolved organic matter; 2.65 Pg C yr^{-1} of the dissolved organic matter that is produced in the surface is remineralized there. The organic matter that leaves the surface is remineralized at depth (we omit the small sediment burial and river input contributions). Our predicted organic matter export is comparable to other work. Recently, *Chavez and Toggweiler* [1995] estimated that global new production is 7.2 Pg C yr^{-1}, a value that is toward the low end of recent estimates they cite that range from 5 to 22 Pg C yr^{-1} [*Chavez and Barber*, 1987; *Martin et al.*, 1987; *Packard et al.*, 1988; *Najjar et al.*, 1992; *Sarmiento et al.*, 1993]. We are not aware of many estimates of global DOC export production; however, our estimate of DOC export is consistent with work by *Yamanaka and Tajika* [1997], who find that DOM export production at 100 m is 3 Pg C yr^{-1}.

Carbonate export from the surface is 1.77 Pg C yr^{-1} of which 1.54 Pg C yr^{-1} is added at depth because of dissolution. The difference, 0.23 Pg C yr^{-1}, represents the burial flux of carbonate and is added back to the surface in order to conserve TA in the model. The model burial flux is in good agreement with other estimates that range between 0.12 and 0.24 Pg C yr^{-1} [*Sarmiento and Sundquist*, 1992; *Milliman*, 1993]. The global $CaCO_3$/POC export ratio is 0.26.

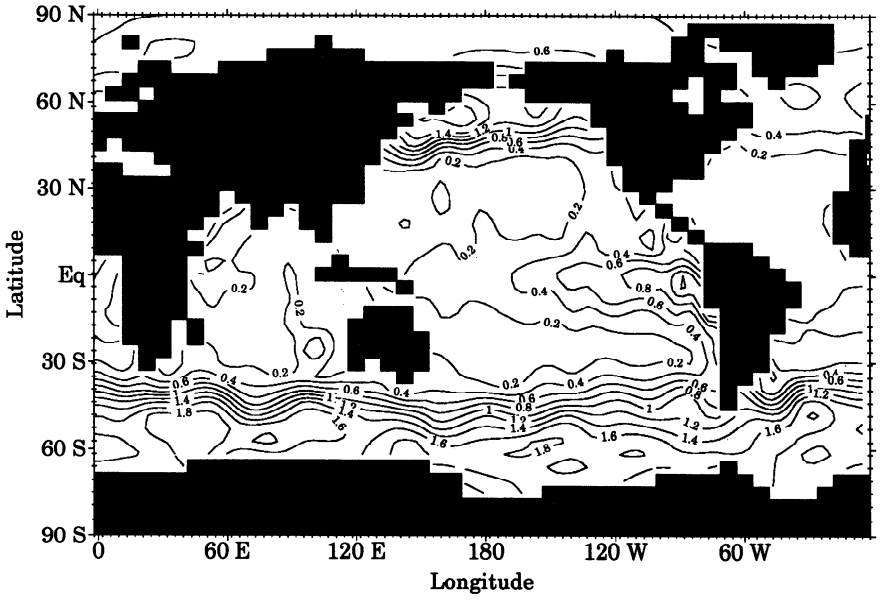

Figure 5. Global annual mean surface phosphate concentration (μmol kg^{-1}). Note the regions of high phosphate concentrations near the equator and in high latitudes.

In a steady state the downward flux of organic matter must be balanced by an equal and opposite transport of DIC. The upward transport requires a steepening of the vertical DIC gradient relative to the solubility model (Figure 4). The surface concentration of DIC is determined primarily by the atmospheric pCO_2, which is fixed at 278.2 μatm for both the solubility model and OBM. Also important is the surface TA, which is reduced from a global average of 2372 μmol kg^{-1} in the solubility model to 2304 μmol kg^{-1} in the OBM. The reduction is a consequence of the combined effect of $CaCO_3$ formation and nitrate removal. Reductions in TA diminish the carbon-holding capacity of water for a given pCO_2. Thus mean surface DIC decreases from 2021 μmol kg^{-1} in the solubility model case to 1968 μmol kg^{-1} in the OBM. This reduction is insufficient to give the vertical gradient of DIC required to balance the organic matter flux. The model therefore achieves the required steepening of the vertical gradient by increasing the deep ocean DIC concentration. The resulting addition of 2537 Pg C to the ocean at steady state is an increase of 6.8% over the solubility model value of 37,477 Pg C.

Level mean DIC concentrations in the OBM are lower than the GEOSECS observations at all depths (Figure 4). Two factors contribute to this. First, the predictions are for a preindustrial ocean so that there is no anthropogenic carbon component. Second, the model's thermocline is too warm by nearly 2°C. This warmer temperature lowers the equilibrium concentration of DIC by approximately 15 μmol kg^{-1}. Adding this carbon to the thermocline would eliminate a large fraction of the difference between the OBM results and the GEOSECS observations. Additional possibilities that could increase deep ocean DIC concentrations include C:P ratios in organic matter that are greater than those used in the OBM (120) and the remineralization of phosphate at shallower depths than carbon.

How does the biological pump affect the sea-air flux? In regions of upwelling and convective mixing the higher deep ocean concentrations and steep vertical gradients will increase the carbon flux to the surface, where it can, in principle, escape to the atmosphere. However, biological uptake at the surface generally strips out the excess deep carbon before escape to the atmosphere can occur. Escape of excess CO_2 to the atmosphere occurs only in regions where biological uptake is inefficient. A good diagnostic of such regions is high surface nutrient concentrations (Figure 5) such as those that occur in the Southern Ocean and tropical and North Pacific. For example, in the Southern Ocean CO_2 efflux from the biological model is large enough to nearly cancel CO_2 uptake from the solubility model (Figure 6). Recall that the biological model result is obtained by subtracting the solubility model from the OBM. The biological model shows the expected escape of CO_2 to the atmosphere in the high nutrient regions of the Southern Ocean, the equator, and the high northern latitudes. Elsewhere there is uptake, as must be the case in order to balance out the global sea-air flux to the steady state value of 0.

If the biological pump operated at 100% efficiency everywhere in the surface ocean, there would be no biological model air-sea CO_2 flux. We approximate the effect of an efficient biological pump by restoring surface phosphate concentrations to zero instead of to the observed phosphate. We refer to this as the "superbiota" simulation. The timescale for restoring is still 100 days so that surface phosphate does not go exactly to zero and can be up to several tenths of a micromolar concentration in areas with intense convection such as the Southern Ocean. Export production in the superbiota model is 2.1 times that in the biological model, and air-sea fluxes are nearly 1/3 that in the biological model (Figure 7). Export production in the Southern Ocean of the superbiota model increases dramatically over that in the biological model because it is a region where the normal model has high surface phosphate concentrations and vertical exchange is large [*Sarmiento and Orr*, 1991].

The contribution of $CaCO_3$ cycling to air-sea CO_2 fluxes is small except in the Southern Ocean (Figure 8) where deep ocean water with elevated TA outcrops at the surface and increases the

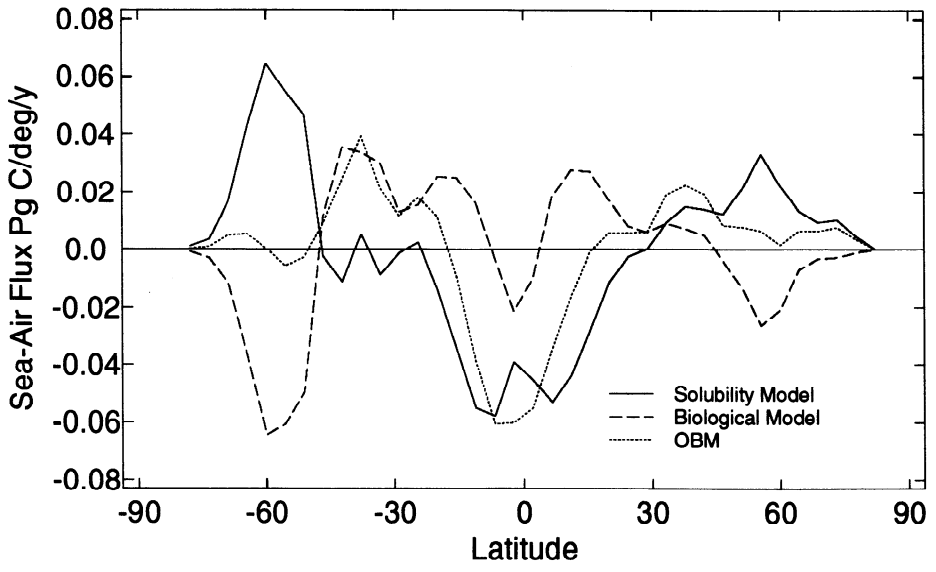

Figure 6. Zonal average CO_2 fluxes for the solubility and biological models and the OBM. Note that in high-latitude regions the solubility and biological model tend to cancel each other, whereas at the equator they tend to reinforce each other.

carbon uptake capacity of the surface water. The higher TA gives a larger carbon holding capacity relative to other regions, resulting in the uptake of atmospheric CO_2 concentrated at 60°S. Much of this excess CO_2 is advected toward the north and escapes to the atmosphere in low surface nutrient (and thus low surface TA) regions quite near to the sink region. Sediments in the Southern Ocean tend to be siliceous rather than carbonaceous [*DeMaster*, 1981]. The abundance of siliceous sediments suggests that silica-based production is greater in the Southern Ocean than in other regions of the world ocean. In future simulations it would probably be more realistic to reduce the production of $CaCO_3$ in the Southern Ocean, but the effect on the sea-air fluxes would be relatively small.

The solubility model and OBM absorb almost identical amounts of anthropogenic carbon (Figure 9 and Table 2) and have a very similar spatial distribution of anthropogenic carbon air-sea fluxes (Figure 10). The greatest uptake of anthropogenic carbon occurs in the Southern Ocean where deep water is ventilated and gas transfer velocities are high [*Sarmiento et al.*, 1992]. The OBM absorbs slightly less anthropogenic carbon than the solubility model because the global mean surface water TA is 68 μmol kg^{-1} less than that in the solubility model, and the carbon uptake capacity of sea water decreases as TA falls.

In 1990 the equatorial region (within ±15° of the equator) of the OBM has an efflux of 0.7 Pg C yr^{-1} to the atmosphere (Table 1) with most of the efflux occurring in the Pacific (0.5 Pg C yr^{-1}). This flux agrees well with data-based estimates [*Takahashi et al.*, 1997] (Figure 11 and column 6 of Table 1). The Northern Hemisphere oceanic fluxes from the OBM and *Takahashi et al.* [1997] also agree to within 0.3 Pg C yr^{-1} (Table 1). In addition, OBM CO_2 fluxes in the North Atlantic [*Sarmiento et al.*, 1995] compare well with the observationally based estimates [*Takahashi et al.*, 1995] and suggest that the OBM can do a reasonable job of predicting air-sea CO_2 fluxes on basinal as well as global scales. However, there are areas with significant differences between OBM and data-based CO_2 fluxes. The OBM has a larger uptake than the *Takahashi et al.* [1997] estimate in the Southern Hemisphere. The patterns within the regions also differ most notably at the equator where the OBM overestimates the efflux of CO_2 at the equator and underestimates the flux elsewhere in the tropical region (Figure 11) relative to Takahashi et al. (Table 1).

Tans et al. [1990] and *Keeling et al.* [1989] also provide estimates of air-sea fluxes with which our model simulations can be compared (Table 1). The first estimate by *Tans et al.* [1990] (column 3 of Table 1), which gives a large equatorial efflux balanced mainly by Southern Hemisphere oceanic uptake in the 1970s and 1980s, is based on observations of sea-air CO_2 pressure differences and a radiocarbon-based gas exchange model. The southward atmospheric transport implied by this distribution of air-sea fluxes was not consistent with the observed north-south gradient in atmospheric CO_2 and the predicted atmospheric transport [*Tans et al.*, 1990]. This inconsistency drove *Tans et al.* [1990] to develop a range of air-sea flux scenarios (column 4 of Table 1) based on a fit of atmospheric pCO_2 observations to predictions from an atmospheric transport model. In these scenarios the asymmetry between Northern and Southern Hemisphere carbon uptake by the ocean is reduced, but so also is the total oceanic uptake. More recent compilations of sea-air CO_2 pressure differences [*Takahashi et al.*, 1995] suggest that the North Atlantic is a larger sink of carbon than was estimated by *Tans et al.* [1990].

Results in Table 1 from the *Keeling et al.* [1989] study are based on an atmospheric transport model constrained by the observed meridional CO_2 gradient. The Keeling et al. results for 1984 suggest that a large equatorial efflux is balanced mainly by Northern Hemisphere uptake (column 5 of Table 1). The large Northern Hemisphere uptake in the *Keeling et al.* [1989] results for 1984 is present also in their preindustrial flux estimates (Table 1). The preindustrial air-sea fluxes in *Keeling et al.* [1989] result

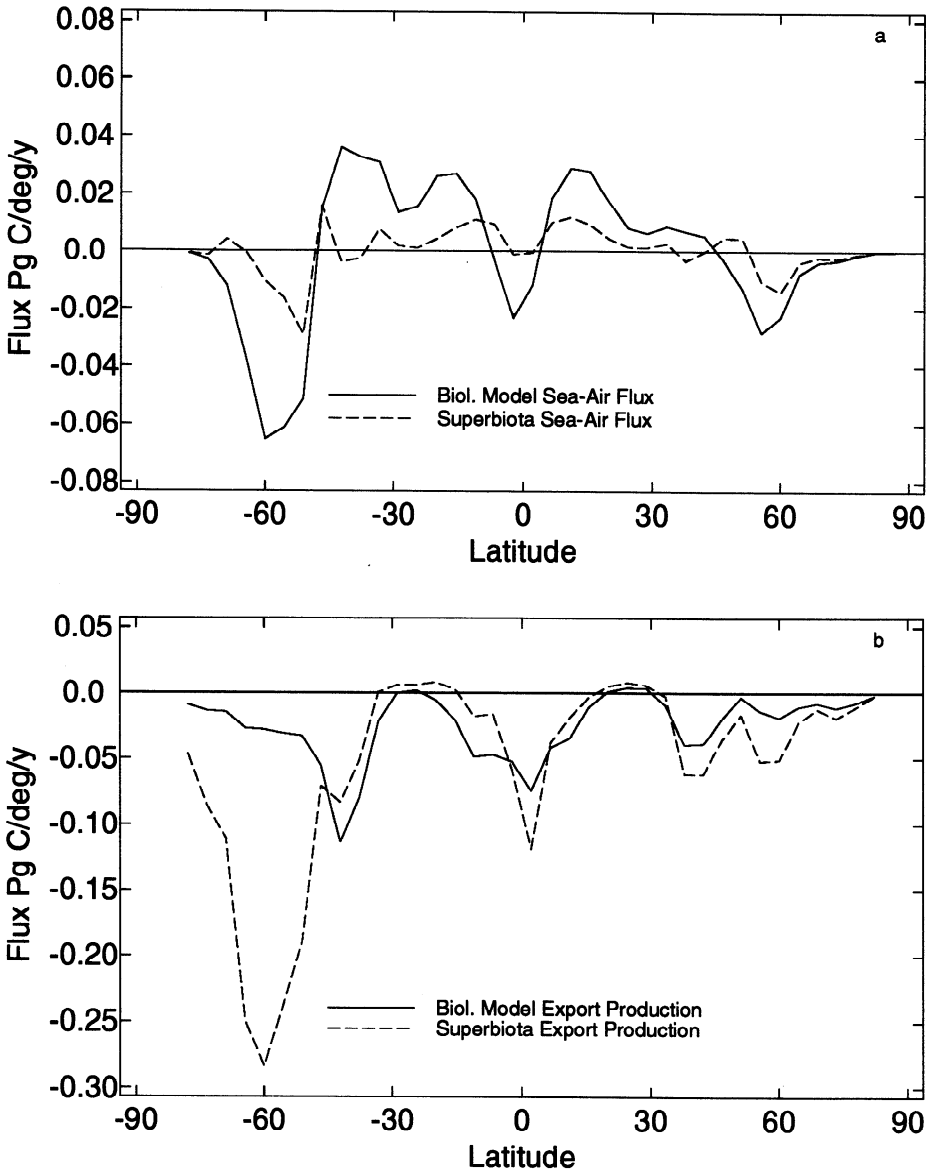

Figure 7. Comparison of export production and air-sea fluxes. Two scenarios are shown. The first scenario shows results from the OBM. The second scenario is based on a biological model with a "superbiota" in the biological pump. In this scenario, phosphate concentrations in the top two levels are restored to zero everywhere at a 100 day timescale. As a result, surface phosphate concentrations are much lower than in the OBM. (a) Air-sea fluxes for the two scenarios shown at the same scale as that in Figure 6. (b) Export production fluxes for the two scenarios; note the different scale compared to Figure 7a. The magnitude of the air-sea flux tends to be much smaller than that of the export production flux in the superbiota scenario. In the extreme case where surface phosphate concentrations were everywhere reduced to zero, there would be no air-sea CO_2 flux due to a "superbiological model," and export production would be even higher.

in a cross-equatorial transport of 0.9 Pg C yr^{-1} and include an ocean efflux of 0.4 Pg C yr^{-1} south of 40°S. These transport and flux estimates differ greatly from the OBM results for the preindustrial era which have essentially no interhemispheric transport of DIC (Figure 3c) and very little efflux of CO_2 from the southern ocean (Figure 6).

5. Interhemispheric Carbon Transport

We now examine in more detail the interhemispheric transport of carbon by the preindustrial ocean because of its importance for the natural "background" global biogeochemical cycle of carbon. Analyses of oceanic data suggest that there was significant southward transport of carbon in the Atlantic Basin [*Broecker and Peng*, 1992; *Keeling and Peng*, 1995]. The preindustrial OBM also predicts a southward cross-equatorial transport of carbon in the Atlantic. However, this is balanced by a northward transport in the Pacific such that globally there is essentially no interhemispheric transport of carbon by the ocean. In the context of our model, interhemispheric transport by the ocean must be driven by a combination of the solubility pump, the biological pump, and gas exchange kinetics. We examine each in turn to as-

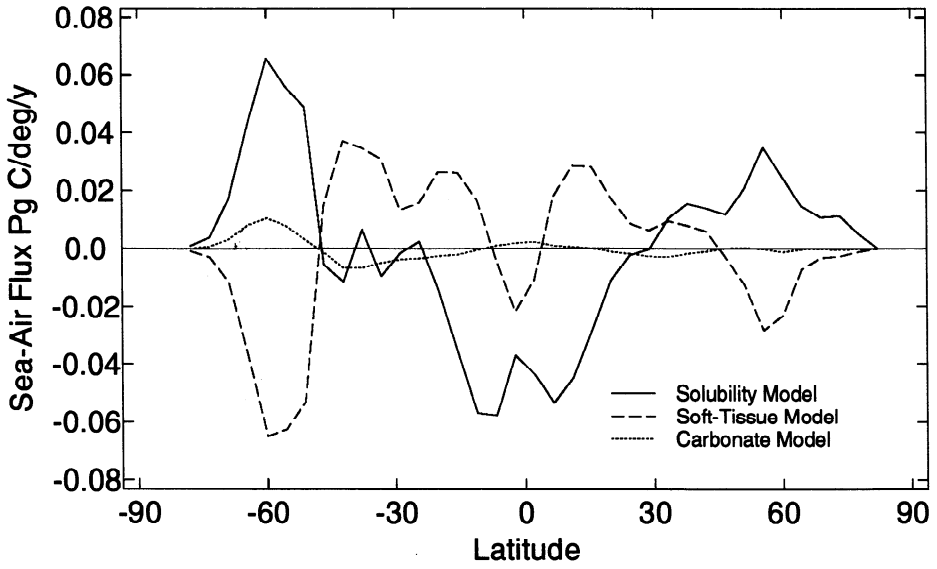

Figure 8. Comparison of air-sea fluxes due to the solubility model, the cycling of organic carbon (soft-tissue model), and the cycling of calcium carbonate (carbonate model). The carbonate model contribution is defined as the difference between the OBM and a run with only the solubility and soft-tissue models.

sess how they affect interhemispheric transport of carbon in a steady state, preindustrial ocean.

Our analysis is complicated by the fact that what we are really interested in is the net oceanic transport of carbon across the Intertropical Convergence Zone (ITCZ) in the atmosphere. The ITCZ marks the position of the interhemispheric transport barrier that slows the atmospheric flux of anthropogenic carbon from the Northern to the Southern Hemisphere. This constraint on the anthropogenic carbon budget would be greatly eased if we could demonstrate that the ocean carries a significant amount of net carbon across the ITCZ. However, the position of the ITCZ varies with the seasons and has an annual mean that is north of the equator. It will probably require a coupled atmosphere-ocean model to examine this issue satisfactorily. The following discussion of our OBM results can only provide some guidance on the processes that control the interhemispheric carbon transport and what types of analysis might help in understanding it.

We showed earlier that the dominant process driving the potential solubility pump in the ocean is the air-sea exchange of heat. Interhemispheric heat transport by the oceans would drive an interhemispheric carbon transport in the potential solubility model. Although there is a large uncertainty in global meridional transport of heat by the ocean [*Talley*, 1984], it seems reasonable to assume that the transport of heat by the global ocean should

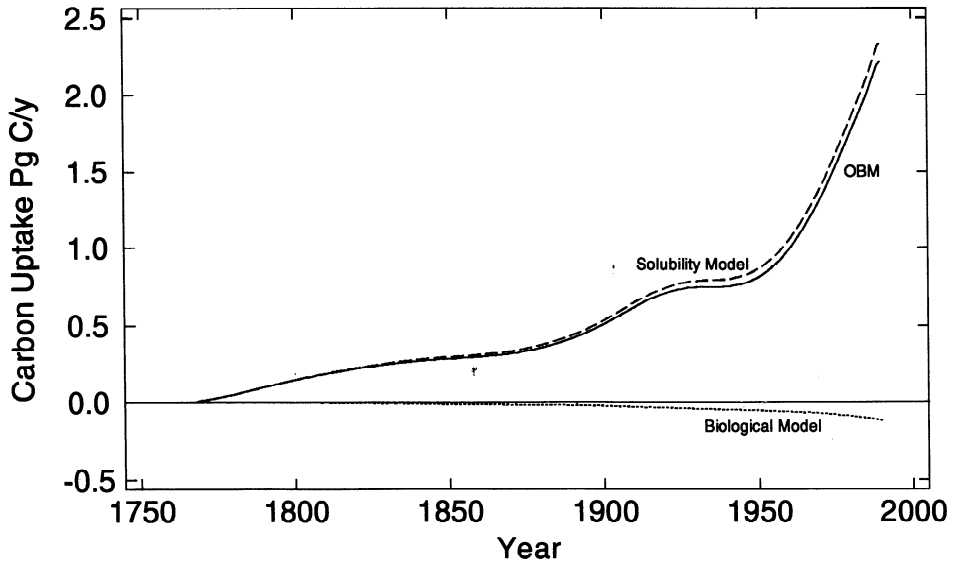

Figure 9. Time series of yearly anthropogenic carbon uptake by the ocean for the solubility and biological models and the OBM.

Table 2. Anthropogenic Carbon Uptake by the Ocean.

	Integrated Uptake 1800:1990, Pg C	Annual Uptake 1980:1989, Pg C y^{-1}
Solubility model	126.89	2.07
Biological model	-6.20	-0.10
OBM	120.69	1.97

change sign somewhere near the equator. The steep gradient in heat transport and the fact that it changes sign near the equator make it difficult to determine the interhemispheric transport with any confidence. The ocean general circulation model transports 0.48 PW of heat southward across the equator but transports 0.19 PW northward at the next grid point to the north, 4.4°N. The model heat transport is consistent with observationally based estimates which show about ±0.3 PW of northward heat transport across the equator, with the sign of northward transport changing within a few degrees of the equator [*Hastenrath*, 1982; *Talley*, 1984; *Semtner and Chervin*, 1992]. In the potential solubility model this heat transport drives 0.39 Pg yr^{-1} of carbon north across the equator and 0.25 Pg yr^{-1} of carbon south at 4.4°N (assuming the water flux is negligible). The only way to increase the cross-equatorial transport of carbon in the potential solubility model would be to increase the cross-equatorial transport of heat. The 0.9 Pg C yr^{-1} estimate [*Keeling et al.*, 1989] of southward cross-equatorial transport by the ocean would require a northward heat transport of nearly 1 PW, which seems unreasonably high compared to the aforementioned ocean models and observations.

The wind speed dependent gas transfer velocity in the solubility model reduces carbon transport north across the equator to 0.22 Pg yr^{-1} (Figure 3). In addition, the latitude where carbon transport changes sign is shifted a few degrees north, from 3° to 6°N.

The addition of the biological pump only slightly alters the global cross-equatorial transport of carbon in the OBM. The transport of biogenic DIC and DOC is closely linked to the transport of nutrients through a Redfield C:P ratio. The only divergence from this that can occur is due to carbonate cycling and gas exchange. As we have shown, the overall impact of carbonate cycling on the global carbon cycle is small (Figure 8) and the same is true of gas exchange. A cross-equatorial transport of carbon might occur if there were a cross-equatorial transport of nutrients. The requirement of conservation of nutrients does not permit such a cross-equatorial transport unless there is an external source or sink. Later we shall mention the possible role of river input and sediment loss of nutrients, which are not included in our OBM.

The addition of the biological pump shifts the point where northward transport of DIC changes sign from 6°N in the solubility model to 3°N in the OBM (Figure 3c). There are 0.28 Pg C yr^{-1} of DIC transported north across the equator and 0.15 Pg C yr^{-1} of DIC transported south at 4.4°N. Total carbon transport, which includes DOC transport, is 0.10 Pg C yr^{-1} north across the equator and is 0.17 Pg C yr^{-1} south at 4.4°N.

Even if there is no net interhemispheric transport of carbon on a global scale, there can be interhemispheric carbon transport within an ocean basin. Such transport is best documented for the Atlantic. *Sarmiento et al.* [1995] showed that in the OBM southward transport of DIC in the Atlantic (0.24 Pg C yr^{-1}) was small compared to observationally based estimates. *Keeling et al.* [1989] suggest that ~0.9 Pg C yr^{-1} were transported south across the equator in the Atlantic. *Broecker and Peng* [1992] estimated that 20 Sv of overturning in the Atlantic carries 0.6 Pg C yr^{-1} southward across the equator. *Keeling and Peng* [1995] estimate that 13 Sv and 0.40±0.18 Pg C yr^{-1} are transported south across the equator and note that DIC transport estimates in the Atlantic Ocean are a function of the amount of overturning. Thus *Keeling and Peng* [1995] lowered *Broecker and Peng*'s [1992] south-

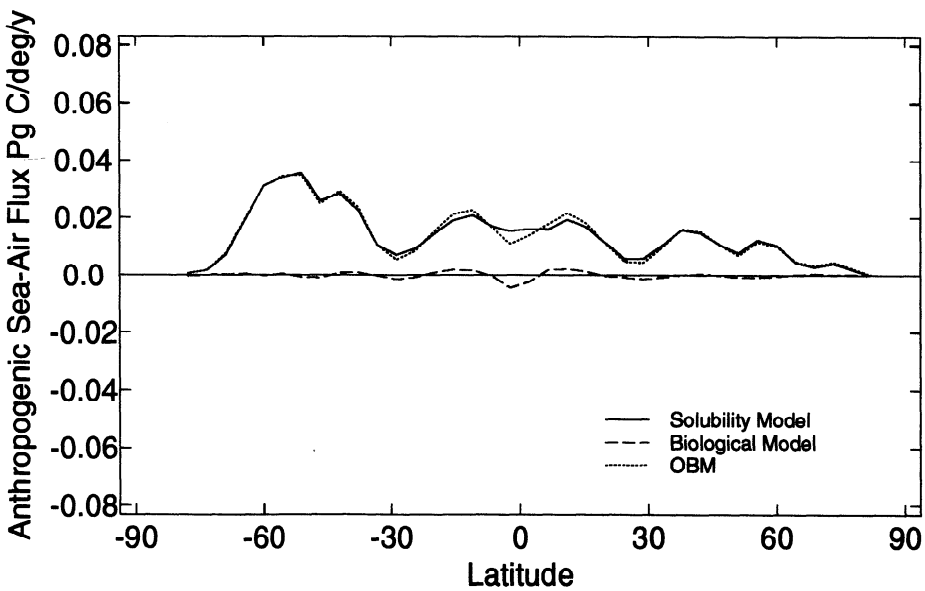

Figure 10. Anthropogenic component of 1990 air-sea carbon flux for the solubility and biological models and the OBM. The net air-sea flux for the biological model is slightly negative because of the reduction of surface total alkalinity and increase in the buffer factor.

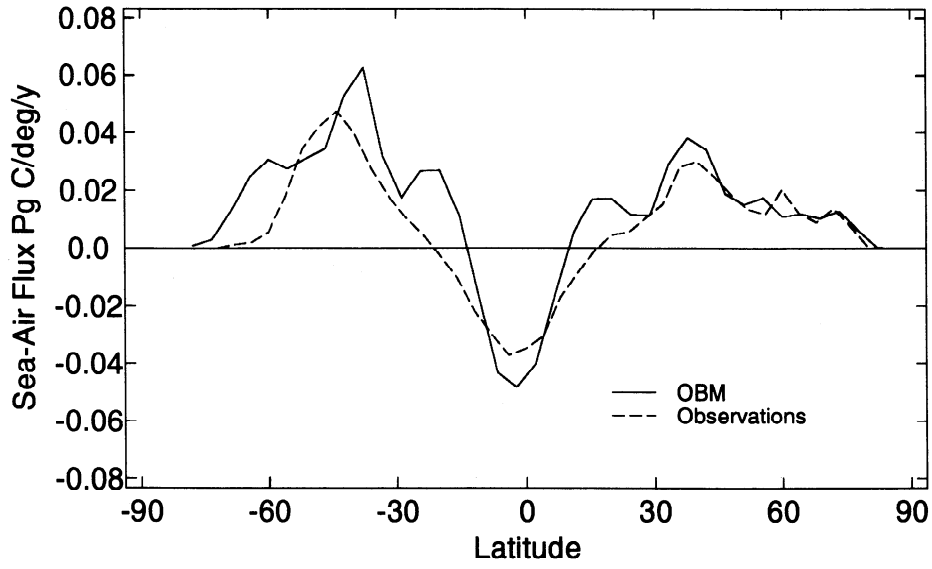

Figure 11. The 1990 OBM CO_2 flux and 1990 CO_2 flux estimated by *Takahashi et al.* [1997] using ΔpCO_2 observations over the last 40 years, an interpolation algorithm, and the *Wanninkhof* [1992] gas transfer velocity.

ward carbon transport estimate of 0.6 Pg C yr^{-1} to 0.4 Pg C yr^{-1} by scaling the 20 Sv of overturning in the Atlantic used by Broecker and Peng to 13 Sv. The Atlantic Ocean of the OBM has a maximum overturning of slightly more than 15 Sv and just over 10 Sv of southward transport across the equator [*Toggweiler et al.*, 1989]. This is lower than other estimates of North Atlantic overturning (compare 13 Sv [*Schmitz and McCartney*, 1993] and 20 Sv [*Broecker et al.*, 1991]), so it is probable that OBM predictions of DIC transport in the Atlantic would be slightly low compared to observationally based estimates. Changing the OBM cross-equatorial transport in the Atlantic to 13 Sv would increase the 0.24 Pg yr^{-1} of DIC transport across the equator to 0.31 Pg C yr^{-1}.

The relatively low overturning in the OBM is consistent with the fact that model heat transport is lower than observations south of 45°N (Figure 12). An increase in the model's Atlantic northward heat transport, and as a result Atlantic overturning, would increase the southward transport of DIC in the Atlantic by the solubility model. However, the fact that the global cross-equatorial ocean heat transport is small suggests that the northward heat transport in the Atlantic is balanced by southward transport elsewhere, which implies that southward carbon trans-

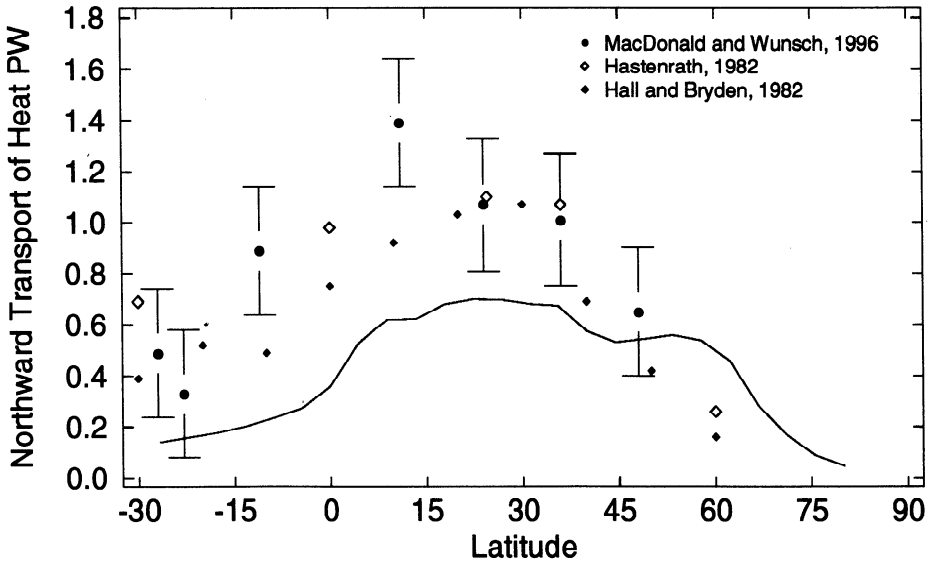

Figure 12. Northward transport of heat in the Atlantic Ocean. The solid lines gives the ocean general circulation model heat transport. The points come from *MacDonald and Wunsch* [1996], *Hastenrath* [1982], and *Hall and Bryden* [1982].

port in the Atlantic due to the solubility pump is balanced elsewhere by northward transport. As a result, increases in Atlantic heat transport would have little effect on the global cross-equatorial transport of heat and DIC. The effect of increased transport and overturning on the biological pump is uncertain. If the biological pump scaled in a manner analogous to the solubility pump, then an increase in model northward heat transport in the North Atlantic should also increase southward transport of DIC in the OBM. With no net interhemispheric transport of phosphate, however, our analysis of the biological model shows that increased Atlantic overturning would not produce global interhemispheric transport of carbon by the biological model and would not support an interhemispheric gradient in atmospheric pCO_2.

River inputs and sediment burial of carbon and nutrients, which are omitted in the OBM, could produce a global interhemispheric flux of carbon through the introduction of a hemispheric asymmetry in carbon and nutrient sources and sinks. We are in the process of adding the influx of carbon to the oceans via rivers [*Meybeck*, 1993; *Ludwig et al.*, 1996]. The global flux of organic plus inorganic carbon to the ocean via rivers is of the order of 1 Pg C yr^{-1} and at steady state should balance carbon burial in ocean sediments. This places a 1 Pg yr^{-1} upper limit on interhemispheric transport of carbon due to asymmetries in carbon and nutrient sources and sinks. However, without a model simulation it is difficult to estimate how an asymmetry in carbon burial would affect the interhemispheric gradient in atmospheric CO_2.

6. Conclusions

Air-sea fluxes of carbon in the potential solubility model closely correlate with thermal fluxes predicted from oceanic heat fluxes and the change in gas solubility with temperature. This is because temperature dependent changes in DIC solubility are the dominant factor in the solubility pump. Oceanic uptake of CO_2 occurs in high-latitude regions where surface waters are cooled, and release occurs in low latitudes where surface waters are warmed. A variable gas transfer velocity causes CO_2 fluxes from the solubility model to differ significantly from CO_2 in the potential solubility model. The differences are caused by the long air-sea equilibration time for CO_2 in the solubility model relative to the residence time of water at the surface.

The biological model produces a large efflux of carbon in the Southern Ocean that essentially cancels the large solubility model influx so that the net air-sea CO_2 flux in the OBM Southern Ocean is small. Efflux of carbon at the equator due to the biological model reinforces the solubility model flux. The preindustrial OBM releases CO_2 to the atmosphere equatorward of 20° and absorbs CO_2 elsewhere except between ~50° and 60°S.

The uptake of anthropogenic carbon by the ocean is mainly controlled by the solubility model. The steady state biological pump slightly decreases the overall uptake of carbon by the OBM becasuse of the lower surface ocean TA relative to the solubility model and the resultant decrease in the carbon capacity of surface waters. The biological pump lowers surface ocean TA because carbonate precipitation lowers TA by a much greater amount than nitrate removal increases TA. The total uptake of anthropogenic carbon by the ocean up to 1990 is 126.9 Pg C for the solubility model and 120.9 Pg C for the OBM.

The carbon inventory produced by the solubility model is 37,477 Pg C. The biological pump adds 2537 Pg C to the ocean so that the total inventory in the OBM is 40,014 Pg C. Level mean profiles of DIC are slightly low compared with GEOSECS observations. Part of the discrepancy is likely due to the warm thermocline in the model.

Zonal mean annual air-sea CO_2 fluxes from the OBM agree quite well with data-based estimates (Figure 11). Global zonal average air-sea CO_2 fluxes in the OBM fall between the estimates of *Keeling et al.* [1989] with a large North Atlantic sink and *Tans et al.* [1990] with a large Northern Hemisphere terrestrial sink. Our estimate of oceanic carbon uptake of 0.34 Pg C yr^{-1} between 18°S and 78°N in the Atlantic agrees with a data-based estimate (0.25-0.53 Pg C yr^{-1} [*Takahashi et al.*, 1995]). The OBM predicts 0.24 Pg yr^{-1} of preindustrial transport of DIC south across the equator in the Atlantic. Despite this southward transport of DIC the OBM has no significant interhemispheric transport on a global scale because of compensating transport in the Indian and Pacific Oceans. The present configuration of the OBM suggests that the preindustrial ocean could not have supported a significant gradient in atmospheric pCO_2.

Appendix: Model Description

The connection between atmospheric CO_2 and oceanic carbon is established via gas exchange. Gas exchange permits air-sea transfer of carbon and is driven by the atmospheric boundary condition. We model this in the usual way as the product of a gas transfer velocity k_W times the atmosphere-ocean difference in CO_2 concentration:

$$f = k_w(1-\gamma_{ice})\left[\alpha(pCO_2)atm - (CO_2)oc\right] \qquad \text{(A1)}$$

The first term in parentheses on the right hand side is a correction for the fraction of ice cover. Inside the brackets are α, the solubility of CO_2; $(pCO_2)_{atm}$, the atmospheric partial pressure corrected to 100% humidity at the temperature of surface water [see *Sarmiento et al.*, 1992; and $(CO_2)_{oc}$, which is the surface ocean concentration of CO_2 found mostly in the hydrolyzed form H_2CO_3. Solving (A1) for f requires specifying or modeling all the terms on the right hand side. Each of these is discussed in turn.

The gas transfer velocity k_W is a function of wind speed U and Schmidt number Sc following the bomb radiocarbon calibrated relationship of *Wanninkhof* [1992]:

$$k_W = 0.39U^2\left(\frac{Sc}{660}\right)^{-0.5} \qquad \text{(A2)}$$

The observational analysis of *Esbensen and Kushnir* [1981] provides the wind speed U. The Schmidt number is a function of temperature [*Jahne et al.*, 1987]. Temperature is obtained from the ocean circulation model. The fraction of sea ice cover γ_{ice} is specified using the observational analysis of *Alexander and Mobley* [1976]. CO_2 solubility α is taken from *Weiss* [1974]. The magnitude of $(pCO_2)_{atm}$ is specified. The preindustrial $(pCO_2)_{atm}$ we use is 278.2 μatm (dry atmosphere value).

Simulation of the atmosphere-ocean carbon distribution requires a set of initial conditions. Previous studies have specified the initial total carbon content and maintained it at a constant value throughout the simulation [e.g. *Maier-Reimer and Hasslemann*, 1987; *Bacastow and Maier-Reimer*, 1990, 1991]. Because of errors in observations and the models, this approach generally leads to a different atmospheric pCO_2 than observed.

An important constraint on the model simulations is that we would like to reproduce the pre-industrial atmospheric pCO_2 content so that we can use the models as an initial condition for simulations of the time history of the anthropogenic transient. One way to do this is to run several simulations with different initial carbon inventories until one is found that gives the desired result. A more simple approach, which we adopt, is to fix atmospheric pCO_2 at its observed value and allow it to invade the ocean. Equilibrium is achieved when the globally integrated net CO_2 sea-air flux is negligible. Our approach guarantees that the final total carbon content obtained at equilibrium will be consistent with the observed preindustrial dry atmosphere pCO_2 of 278.2 μatm.

The set of chemical reactions that play a role in determining the concentration of $(CO_2)_{oc}$ are solved using a procedure analogous to that of *Peng et al.* [1987] with equilibrium constants as summarized in Table A1. We use model values of DIC, TA, temperature, and salinity to solve the carbon system equations. The values of these tracers are found using the ocean circulation model as described below.

The biogeochemical tracer equation solved by the ocean circulation model is

$$\Gamma(C) = J(C) \tag{A3}$$

where the time rate of change and transport operator $\Gamma(C)$ is

$$\Gamma(C) = \frac{\partial C}{\partial t} + \mathbf{V}\cdot\nabla C - \nabla_h\cdot(\mathbf{K}_h\nabla_h C) - \frac{\partial}{\partial z}\left(\frac{K_v}{\delta}\frac{\partial C}{\partial z}\right) \tag{A4}$$

and J represents the combination of all in situ sources minus sinks. At steady state, (A3) states that the transport divergence defined by (A4) is equal to the in situ sources minus sinks. The tracer concentration is represented by C, $\mathbf{V}$ is velocity, ∇ is the divergence operator, and $\mathbf{K}$ is the diffusion tensor. The diffusion term is separated into a horizontal (subscript h) and vertical (subscript v) component. The parameter δ is 1, except when two adjacent layers are gravitationally unstable with respect to each other, in which case the two layers are homogenized (i.e., δ=0).

Ocean circulation is predicted using wind stress fields taken from *Hellerman and Rosenstein* [1983] and surface heat and salinity fluxes obtained by damping model temperature and salinity toward the climatic annual means of *Levitus* [1982] [see also *Toggweiler et al.*, 1989].

Solving (A3) requires specifying J and the boundary and initial conditions for the biogeochemical tracers. We describe these in section A1 on the sources and sinks in the solubility model and the OBM. We end with a discussion of the virtual flux that we include in the model to account for the approximations introduced by the model's rigid lid.

Table A1. Equilibrium Constants and Concentrations Used for Carbon Chemistry Calculations

Equilibrium constant or fractionation factor	Reference
Carbon K_1, K_2	[*Goyet and Poisson*, 1989]
Borate K	[*Dickson*, 1990]
Silicate K	[*Sjoberg et al.*, 1981]
Phosphoric acid K_1, K_2, K_3	[*Dickson and Riley*, 1979b]
Water K	[*Dickson and Riley*, 1979a]
Term	**Source**
Total borate[a]	S‰x11.88 μmol kg^{-1} ‰$^{-1}$
Total phosphate	2.15 μmol kg^{-1}
Total silica[b]	S‰x3.143 μmol kg^{-1} ‰$^{-1}$
Total sulfate[b]	S‰x0.8067 mmol kg^{-1} ‰$^{-1}$
Total fluorine[b]	S‰x1.981 μmol kg^{-1} ‰$^{-1}$
β_{SO_4}	[*Khoo et al.*, 1977]
β_{HF}	[*Dickson and Riley*, 1979b]
Ionic strength	I = 1.00311S/50.378

a. Based on boron/chlorinity relationship of *Uppström* [1974].
b. Based on mean water concentrations given in *Quinby-Hunt and Turekian* [1983].

A1. Solubility model

The final DIC distribution is independent of the initial DIC because the ocean equilibrates with an atmospheric CO_2 reservoir of infinite size. There are no internal sources or sinks so that $\Gamma(C)$ = 0. Dissolved organic carbon concentrations are zero. Total alkalinity is a linear function of salinity. Air-sea carbon fluxes are based on the differences between $\alpha(CO_2)_{atm}$ and $(CO_2)_{oc}$ calculated from surface ocean temperature, salinity, DIC, and TA and the calculated gas transfer velocity (see (A1)).

A2. OBM

The OBM includes processes associated with the solubility and biological models. The biological model is based on the cycling of phosphate. Our modeling of phosphate is derived from earlier work in our group [*Sarmiento et al.*, 1988; *Najjar et al.*, 1992; *Anderson and Sarmiento*, 1995] and modified for this particular study. The phosphate conservation equation includes terms for both particulate and dissolved material

$$\Gamma(PO_4^{3-}) = -J(POP) - \Gamma(LDOC)/r_{C:P} \tag{A5}$$

The first term on the right hand side of (A5) represents the impact of particulate organic phosphate (POP) cycling on the phosphate distribution. The second term accounts for the cycling of labile dissolved organic phosphorus, which is obtained from LDOC using the stoichiometric ratio of 120:1 obtained by *Anderson and Sarmiento* [1994].

The distribution of POP is not solved explicitly. Rather, the POP sources minus sinks required for (A5) are specified as follows:

$$J(POP) = (1-\delta_z)(1-\sigma)\Pi - \delta_z\frac{\partial F_{POP}}{\partial z} \tag{A6a}$$

$$F_{POP} = F_{z_e}(z/z_e)^{-0.858} \tag{A6b}$$

$$F_{z_e} = (1-\sigma)\int_0^{z_e}\Pi dz \tag{A6c}$$

$$\Pi = \delta_b\left[[PO_4^{3-}] - [PO_4^{3-}]_{observed}\right]/\tau \tag{A6d}$$

The first term on the right-hand side of (A6a) is production of POP by biological synthesis in the euphotic zone. The parameter δ_z is set to 0 in the upper two "euphotic" layers of the model and has a value of 1 below that. Production of dissolved and particulate organic phosphorus in the euphotic zone Π is determined by

requiring that model predicted phosphate be relaxed towards the observed phosphate distribution as specified by (A6d). Half the new production is put into particles, and half is put into labile dissolved organic matter following *Anderson and Sarmiento* [1995]. The fraction of the total production that goes into POP is specified by $(1-\sigma) = 0.5$. To prevent negative, production the parameter δ_b in (A6d) is 1 when the term inside the brackets of the first term is positive and is 0 otherwise. The timescale τ is 100 days.

The second term on the right-hand side of (A6a) is remineralization of POP which occurs only below 119 m (the top of the third level) where δ_z is set to 1. F_{POP} is the flux of POP as a function of depth as specified by (A6b) obtained from sediment trap observations by *Martin et al.* [1987]. Remineralization of POP occurs immediately below where it is formed. The flux of POP at the base of the euphotic zone (z_e = 119 m) specified by (A6c) is equal to the vertically integrated production of POP within the euphotic zone.

The cycling of phosphate also requires simulating the distribution of labile dissolved organic carbon LDOC:

$$\Gamma(LDOC) = r_{C:P}(1-\delta_z)\sigma\Pi - \kappa\delta_{do}[LDOC] \qquad \text{(A7)}$$

The first term of (A7) is LDOC production in the euphotic zone above 119 m, and the second term is LDOC remineralization. The δ_{do} term is 1 when $[LDOC]>0$ and 0 when $[LDOC]\leq 0$. Note that $\sigma = 0.5$; that is, 50% of the production of organic matter goes into LDOC. LDOC is transported away from the region of production as a passive tracer following the water motion. Remineralization occurs as a first-order decay process at all depths. The decay constant is set each time step to conserve total LDOC at a global average of 4.2 μM. The global average value is based on an assumption that average upper ocean DOC concentration is 35 μM greater than the deep ocean, that deep ocean DOC is all refractory and long-lived, and that the upper ocean volume is 12% of the total ocean volume (35x0.12=4.2). The decay constant obtained after equilibration of the model is 1/11.2 yr^{-1}.

The total alkalinity TA equation for the OBM accounts for the cycling of nitrate and carbonate due to the biological model

$$\Gamma(TA) = -r_{N:P}\Gamma(PO_4^{3-}) - 2J(CaCO_3) \qquad \text{(A8)}$$

The first term on the right-hand side of (A8) accounts for the effect of nitrate ion on TA, with $r_{N:P} = 16$. The second term on the right-hand side accounts for the effect of carbonate cycling on TA. The sources minus sinks of $CaCO_3$ required for solving (A8) are obtained from

$$J(CaCO_3) = \delta_a R_{Ca:P} J(POP) \qquad \text{(A9a)}$$

$$R_{Ca:P} = 0.5\left(\overline{A}_{model} - \overline{A}_{observed}\right) / \overline{J(POP)} \qquad \text{(A9b)}$$

$$A = \left(TA + r_{N:P}\Delta t\left(\kappa[DOP] + J(POP)\right)\right)(S_O/S) \qquad \text{(A9c)}$$

$$\overline{A} = \iiint(A)\,dx\,dy\,dz \,/\, \iiint dx\,dy\,dz \qquad \text{(A9d)}$$

We specify $J(CaCO_3)$ using a quasi-diagnostic approach based on forcing $\overline{A}_{model}$, the salinity normalized, global horizontal mean TA given by (A9d), toward the observed mean from GEOSECS observations, $\overline{A}_{observed}$, at each depth level (see numerator of the right-hand side of (A9b)), correcting first for the effect of nitrate cycling and salinity variations as specified by (A9c). $R_{Ca:P}$ is the ratio of the global horizontal mean sources minus sinks of $CaCO_3$ to the global horizontal mean of sources minus sinks of POP, $J(POP)$ for each level as in (A9b). $R_{Ca:P}$ at each level is used in combination with the local production or remineralization of POP to determine the local distribution of $J(CaCO_3)$.

The δ_a parameter in (A9a) is 1 unless any of several conditions are violated, in which case $0 \leq \delta_a < 1$. The conditions that must be satisfied are the following. (1) In levels 1 and 2 there must be formation of $CaCO_3$, that is, $\overline{A}_{model} > \overline{A}_{observed}$. (2) In level 3-12 there can only be dissolution of $CaCO_3$, that is, $\overline{A}_{model} < \overline{A}_{observed}$. If either of these conditions is violated at any level, δ_a is set to 0 for that level. (3) A final condition is that the vertically integrated dissolution of $CaCO_3$ at any given latitude and longitude must be less than or equal to the production in the top levels. This condition is checked beginning with the third layer and adding one layer at a time moving downward. As long as the integrated dissolution is less than the production, δ_a is set to 1. If a level is reached where the integrated dissolution exceeds the production, then δ_a is set to a fraction between 0 and 1, such that the total dissolution equals exactly the production at the surface and all deeper levels have δ_a set to 0. Any excess $CaCO_3$ production is assumed to be lost to the sediments and replaced by river inflow. The total excess production is put into a pool that is replaced by an alkalinity source to the photic zone as a function of volume.

With the cycling of organic matter and calcium carbonate specified, we can now write the conservation equation for DIC

$$\Gamma(DIC) = r_{C:P}\Gamma(PO_4^{3-}) - J(CaCO_3) \qquad \text{(A10)}$$

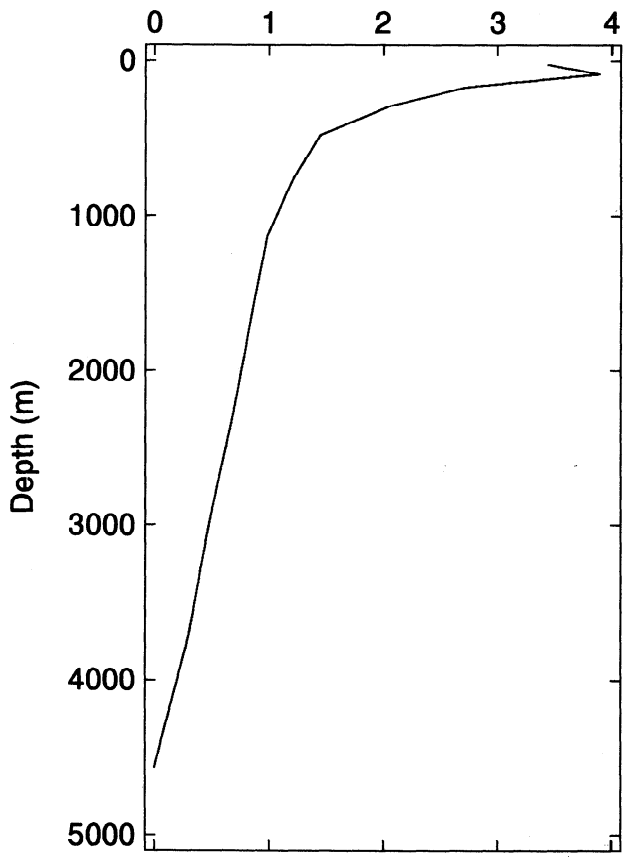

Figure A1. Global $CaCO_3/C_{org}$ flux ratio as a function of depth.

The first term on the right reflects the cycling of particulate and labile dissolved organic carbon; the second term accounts for the cycling of calcium carbonate, $r_{C:P} = 120$.

The way we parameterize $CaCO_3$ cycling has the advantage that organic carbon to carbonate production ratios do not need to be specified a priori and that we do not need to solve for sedimentary diagenesis of $CaCO_3$ and organic matter. The final vertical profile of TA that our model predicts is almost exactly equal to the global TA averaged on horizontal levels. A possible drawback of our approach is that we ignore the existence of the aragonite and calcite saturation horizons and the fact that these are deeper in the Atlantic than in the Indian and Pacific Oceans. However, there is evidence that $CaCO_3$ dissolution occurs above these horizons in all the ocean basins [e.g., *Anderson and Sarmiento*, 1994], perhaps due to the influence of CO_2 produced by organic matter remineralization in sediments [e.g., *Emerson and Bender*, 1981; *Archer et al.*, 1989]. Our model develops the upward slope of the carbonate saturation horizon that is observed to occur in going from the Atlantic to the Indian and Pacific Oceans. However, our slope is less than the observations because of the fact that our dissolution function does not take this slope into consideration and will thus tend to have higher dissolution in the Atlantic. We are presently working on a better parameterization of TA that will be based on river inputs of alkalinity and restoring toward TA observations.

We note that the contribution of nitrate to TA is keyed directly to that of phosphate in our model. This ignores denitrification and nitrogen fixation. While these are generally considered to be small, we plan in the future to model the nitrate directly so these processes can be taken into account.

Figure A1 shows a plot of the POC to $CaCO_3$ flux ratio. The $CaCO_3$ exported from the surface ocean is 1/5.2 times the POC export. Dissolution of $CaCO_3$ is a significant fraction of organic matter remineralization at all depths in the model below the euphotic zone except level 10 at 2935 m, where no dissolution occurs because of the fact that the model predicted horizontally averaged TA is slightly higher than the observed concentration.

A3. Virtual flux

In addition to air-sea gas fluxes there is a "virtual flux" at the surface of the ocean for each passive tracer that results from the way that precipitation and evaporation are handled in the model. Freshwater fluxes are not modeled explicitly in the primitive equation ocean circulation model because the rigid lid approximation requires that ocean volume be conserved at each grid box. Instead, the model accounts for freshwater fluxes by modifying salinity via a restoring term. The salinity flux implies a freshwater flux that would concentrate or dilute other tracers. The virtual flux alters tracer concentrations via a linear function of the salinity restoring flux. The virtual flux should not be confused with the air-sea flux of a tracer. One can think of the virtual flux as an approximation to the additional tracer transport that would exist within the ocean if the freshwater atmosphere-ocean fluxes and the corresponding oceanic transports were modeled explicitly. We are convinced that the virtual flux correction forces the model-predicted air-sea fluxes closer to what they would be if the water fluxes were handled explicitly, but we have no definitive proof for this conviction.

We derive the correction for the virtual flux in the following manner. Let the mass of salt in a grid box be M. A change in salinity ΔS for a grid box is caused by a change in salt mass ΔM in a rigid-lid model (*rigid*) or a change in volume, ΔV, in a model with explicit freshwater fluxes (*fwf*):

$$\Delta S_{rigid} = \frac{M+\Delta M}{V\rho} - \frac{M}{V\rho} = \frac{\Delta M}{V\rho} \tag{A11}$$

$$\Delta S_{fwf} = \frac{M}{(V+\Delta V)\rho} - \frac{M}{V\rho} \tag{A12}$$

where V is volume and ρ is density (we assume a negligible change in ρ). We want the two ΔS terms to be equal, that is,

$$\frac{M+\Delta M}{V\rho} - \frac{M}{V\rho} = \frac{M}{(V+\Delta V)\rho} - \frac{M}{V\rho} \tag{A13a}$$

$$\frac{M+\Delta M}{M} = \frac{V}{V+\Delta V} \tag{A13b}$$

For a passive tracer with concentration C the change in concentration ΔC associated with the implied change in volume is

$$\Delta C = T\left(\frac{1}{V} - \frac{1}{V+\Delta V}\right)$$

$$= CV\left(\frac{V+\Delta V}{V} - \frac{V}{V(V+\Delta V)}\right) = C\left(\frac{V}{V+\Delta V} - 1\right) \tag{A14}$$

where T is the mass of tracer. In the rigid-lid model the salinity flux is given by a salinity restoring term, $\gamma(S^*-S)\Delta z$, based on a reciprocal time constant γ, the difference between model salinity S and observed salinity S^* and the thickness of the surface layer Δz. This gives a change in surface box salinity of $\Delta S = \gamma(S^*-S)\Delta t$. For each time step the change in mass, $\Delta M = V\Delta S\rho$, is just $V\gamma(S^*-S)\rho\Delta t$. We find the change in C consistent with the change in salinity and implied change in volume using this relation and (A14) and substituting for $V/(V+\Delta V)$ using (A13b)

$$\Delta C = C\left(\frac{M+\Delta M}{M} - 1\right) = C\frac{\Delta M}{M}$$

$$= C\frac{V\gamma(S^*-S)\rho\Delta t}{S\rho V} = \frac{C\gamma(S^*-S)\Delta t}{S} \tag{A15}$$

The virtual flux, $C\gamma(S^*-S)\Delta z/S$, is the flux of C that is needed to change tracer concentrations in a manner consistent with the implied water flux. Because of the high concentration of DIC and TA in the ocean and their low variability relative to their concentration, the amount of carbon and TA that is transferred from one

Table A2. Constants for Virtual Flux Calculation

Tracer	Value
S'	34.742‰
DIC'	2052.05 μM
$DI^{13}C'$	22.83 μM
PO_4'	0.53 μM
DOC'	50 μM
$DO^{13}C'$	0.544 μM
O_2'	247.81 μM
$^{18}O'$	0.505 μM
TA'	2368.76 μeq L^{-1}

location to another by the virtual flux is comparable in magnitude to the explicit flux carried by the model circulation.

This derivation assumes that C and S in the virtual flux equation are local values. The use of local values could be a problem because although $\int(F_g + F_v)dA = 0$ will be true at steady state, there is no guarantee that $\int F_g dA = \int F_v dA = 0$ due to a correlation between C and S. Here F_g is the tracer air-sea gas flux, F_v is the virtual flux, and A is area. We therefore use constants S' and C' (Table A2) in the virtual flux ($F_v = C' \gamma(S^*-S)\Delta z/S'$) to insure that $\int F_g dA = 0$ when the global average salinity flux is zero.

Acknowledgments. The development of the OBM was supported at various times by the following grants to Princeton University: Sea Grant via the New Jersey Marine Sciences Consortium (R/M-2), EPRI (RP8011-17 and RP8020-04), DOE (DE-FG02-90ER61052), NSF (OCE-9012333 and OCE-9314707), and NOAA (NA56GP0439). We also gratefully acknowledge computer support from GFDL/NOAA through J. Mahlman.

References

Alexander, R. C., and R. L. Mobley, Monthly average sea surface temperatures and ice pack limits on a 1° global grid, *Mon. Weather Rev.*, *104*, 143-148, 1976.

Anderson, L. A., and J. L. Sarmiento, Redfield ratios of remineralization determined by nutrient data analysis, *Global Biogeochem. Cycles*, *8*, 65-80, 1994.

Anderson, L. A., and J. L. Sarmiento, Global ocean phosphate and oxygen simulations, *Global Biogeochem. Cycles*, *9*, 621-636, 1995.

Archer, D., S. Emerson, and C. Reimers, Dissolution of calcite in deep-sea sediments: *p*H and 0_2 microelectrode results, *Geochim. Cosmochim. Acta*, *53*, 2831-2845, 1989.

Bacastow, R. B., and E. Maier-Reimer, Ocean-circulation model of the carbon cycle, *Clim. Dyn.*, *4*, 95-125, 1990.

Bacastow, R., and E. Maier-Reimer, Dissolved organic carbon in modeling oceanic new production, *Global Biogeochem. Cycles*, *5*, 71-85, 1991.

Bacastow, R. B., C. D. Keeling, T. J. Lueker, M. Wahlen, and W. G. Mook, The ^{13}C Suess effect in the world surface oceans and its implications for oceanic uptake of CO2: Analysis of observations at Bermuda, *Global Biogeochem. Cycles*, *10*, 335-346, 1996.

Banse, K., False advertising in the greenhouse?, *Global Biogeochem. Cycles*, *5*, 305-307, 1991.

Broecker, W. S., Keeping global change honest, *Global Biogeochem. Cycles*, *5*, 191-192, 1991.

Broecker, W. S., and T.-H. Peng, Interhemispheric transport of carbon dioxide by ocean circulation, *Nature*, *356*, 587-589, 1992.

Broecker, W. S., and T.-H. Peng, Stratospheric contribution to the global bomb radiocarbon inventory: Model versus observation, *Global Biogeochem. Cycles*, *8*, 377-384, 1994.

Broecker, W. S., A. Virgilio, and T. H. Peng, Radiocarbon age of waters in the deep Atlantic revisited, *Geophys. Res. Lett.*, *18*, 1-3, 1991.

Chavez, F. P., and R. T. Barber, An estimate of new production in the equatorial Pacific, *Deep Sea Res., Part A*, *34*, 1229-1243, 1987.

Chavez, F. P., and J. R. Toggweiler, Physical estimates of global new production: The upwelling contribution, in *Upwelling in the Ocean: Modern Processes and Ancient Records*, edited by C. P. Summerhayes et al., pp. 313-320, John Wiley, New York, 1995.

DeMaster, D. J., The supply and accumulation of silica in the marine environment, *Geochim. Cosmochim. Acta*, *45*, 1715-1732, 1981.

Dickson, A. G., Thermodynamics of the dissociation of boric acid in synthetic seawater from 273.15 to 318.15 K, *Deep Sea Res., Part A*, *37*, 755-766, 1990.

Dickson, A. G., and J. P. Riley, The estimation of acid dissociation constants in seawater media from potentiometric titrations with strong base, I, The ionic product of water - K_W, *Mar. Chem.*, *7*, 89-99, 1979a.

Dickson, A. G., and J. P. Riley, The estimation of acid dissociation constants in seawater media from potentiometric titrations with strong base, II, The dissociation of phosphoric acid, *Mar. Chem.*, *7*, 101-109, 1979b.

Emerson, S., and M. Bender, Carbon fluxes at the sediment-water interface of the deep-sea: calcium carbonate preservation, *J. Mar. Res.*, *39*, 139-162, 1981.

Esbensen, S. K., and Y. Kushnir, The heat budget of the global ocean: An atlas based on estimates from surface marine observations, *Clim. Res. Inst. Rep.*, *29*, Oregon State Univ., Corvallis, 1981.

Fasham, M. J. R., J. L. Sarmiento, R. D. Slater, H. W. Ducklow, and R. Williams, A seasonal three-dimensional ecosystem model of nitrogen cycling in the North Atlantic euphotic zone: A comparison of the model results with observation from Bermuda Station "S" and OWS "India", *Global Biogeochem. Cycles*, *7*, 379-415, 1993.

Follows, M. J., R. G. Williams, and J. C. Marshall, The solubility pump of carbon in the subtropical gyre of the North Atlantic, *J. Mar. Res.*, *54*, 605-630, 1996.

Francey, R. J., P. P. Tans, C. E. Allison, I. G. Enting, J. W. C. White, and M. Trolier, Changes in oceanic and terrestrial carbon uptake since 1982, *Nature*, *373*, 326-330, 1995.

Friedli, H., H. Lötscher, H. Oeschger, U. Siegenthaler, and B. Stauffer, Ice core record of the $^{13}C/^{12}C$ ratio of atmospheric carbon dioxide in the past two centuries, *Nature*, *324*, 237-238, 1986.

Goyet, C., and A. Poisson, New determination of carbonic acid dissociation constants in seawater as a function of temperature and salinity, *Deep Sea Res., Part A*, *36*, 1635-1654, 1989.

Hall, M. M. and H. L. Bryden, Direct estimates and mechanisms of ocean heat transport, *Deep-Sea Res., Part A*, *29*, 339-359, 1982.

Hastenrath, S., On meridional heat transports in the World Ocean, *J. Phys. Oceanogr.*, *12*, 922-927, 1982.

Heimann, M., and E. Maier-Reimer, On the relations between the oceanic uptake of CO_2 and its carbon isotopes, *Global Biogeochem. Cycles*, *10*, 89-110, 1996.

Hellerman, S., and M. Rosenstein, Normal monthly wind stress over the world ocean with error estimates, *J. Phys. Oceanogr.*, *13*, 1093-1104, 1983.

Hesshaimer, V., M. Heimann, and I. Levin, Radiocarbon evidence for a smaller oceanic carbon dioxide sink than previously believed, *Nature*, *370*, 201-203, 1994.

Jahne, B., G. Heinz, and W. Dietrich, Measurements of the diffusion coefficients of sparingly soluble gases in water, *J. Geophys. Res.*, *92*, 10,767-10,776, 1987.

Joos, F., Bomb radiocarbon: Imbalance in the budget, *Nature*, *370*, 181-182, 1994.

Joos, F., and M. Bruno, Long-term variability of the terrestrial and oceanic carbon sinks and the budgets of the carbon isotopes ^{13}C and ^{14}C, *Global Biogeochem. Cycles*, *12*, 277-296, 1998.

Keeling, C. D. and T. P. Whorf, Mauna Loa, in *Trends '91: A Compendium of Data on Global Change*, edited by T. A. Boden, R. J. Sepanski, and F. W. Stoss, pp.12-14, Carbon Dioxide Info. Anal. Cent., Oak Ridge Nat. Lab., Oak Ridge, Tenn., 1991.

Keeling, C. D., S. C. Piper, and M. Heimann, A three-dimensional model of atmospheric CO_2 transport based on observed winds, 4, Mean annual gradients and interannual variations, in *Aspects of Climate Variability in the Pacific and the Western Americas Geophys. Monogr. Ser.*, vol. 55, pp. 305-363, AGU, Washington D. C., 1989.

Keeling, C. D., T. P. Whorf, M. Wahlen, and J. van der Plicht, Interannual extremes in the rate of rise of atmospheric carbon dioxide since 1980, *Nature*, *375*, 666-670, 1995.

Keeling, R. F., and T.-H. Peng, Transport of heat, CO_2 and O_2 by the Atlantic's thermohaline circulation, *Philos. Trans. R. Soc. London, Ser. B*, *348*, 133-142, 1995.

Keeling, R. F., R. P. Najjar, M. L. Bender, and P. P. Tans, What atmospheric oxygen measurements can tell us about the global carbon cycle, *Global Biogeochem. Cycles*, *7*, 37-67, 1993.

Khoo, K. H., R. W. Ramette, C. H. Culberson, and R. G. Bates, Determination of hydrogen ion concentrations in seawater from 5 to 40°C: Standard potentials at salinities from 20 to 45‰, *Analytic. Chem.*, *49*, 29-34, 1977.

Kurz, K. D., and E. Maier-Reimer, Iron fertilization of the austral ocean-The Hamburg model assessment, *Global Biogeochem. Cycles*, *7*, 229-244, 1993.

Levitus, S., Climatological atlas of the World Ocean, *NOAA Prof. Pap.*, *13*, Natl. Ocean. and Atmos. Admin., Silver Spring, Md., 1982.

Longhurst, A. R., A reply to Broecker's charges, *Global Biogeochem. Cycles*, *5*, 315-316, 1991.

Ludwig, W., J.-L. Probst, and S. Kempe, Predicting the oceanic input of

organic carbon by continental erosion, *Global Biogeochem. Cycles*, *10*, 23-41, 1996.

Macdonald, A. M., and C. Wunsch, Oceanic estimates of global ocean heat transport, in *1996 US WOCE Report*, 48pp., U. S. World Ocean Circ. Exp. Off., College Station, Tex., 1996.

Maier-Reimer, E., Geochemical cycles in an ocean general circulation model: Preindustrial tracer distributions, *Global Biogeochem. Cycles*, *7*, 645-677, 1993.

Maier-Reimer, E., and R. Bacastow, Modeling of geochemical tracers in the ocean, in *Climate-Ocean Interaction*, edited by M. E. Schlesinger, pp. 233-267, Kluwer Acad., Norwell, Mass., 1990.

Maier-Reimer, E., and K. Hasslemann, Transport and storage of CO_2 in the ocean - An inorganic ocean-circulation carbon cycle model, *Clim. Dyn.*, *2*, 63-90, 1987.

Martin, J. H., G. A. Knauer, D. M. Karl, and W. W. Broenkow, VERTEX: Carbon cycling in the northeast Pacific, *Deep Sea Res., Part A*, *34*, 267-285, 1987.

Meybeck, M., Riverine transport of atmospheric carbon: Sources, global typology and budget, *Water Air Soil Pollut.*, *70*, 443-463, 1993.

Milliman, J. D., Production and accumulation of calcium carbonate in the ocean: Budget of a nonsteady state, *Global Biogeochem. Cycles*, *7*, 927-957, 1993.

Najjar, R. G., Marine biogeochemistry, in *Climate System Modeling*, edited by K. E. Trenberth, pp. 241-280, Cambridge Univ. Press, New York, 1992.

Najjar, R. G., J. L. Sarmiento, and J. R. Toggweiler, Downward transport and fate of organic matter in the oceans: Simulations with a general circulation model, *Global Biogeochem. Cycles*, *6*, 45-76, 1992.

Neftel, A., E. Moor, H. Oeschger, and B. Stauffer, Evidence from polar ice cores for the increase in atmospheric CO_2 in the past two centuries, *Nature*, *315*, 45-47, 1985.

Orr, J. C., Accord between ocean models predicting uptake of anthropogenic CO_2, *Water Air Soil Pollut.*, *70*, 465-481, 1993.

Pacanowski, R., K. Dixon, and A. Rosati, The G.F.D.L. modular ocean model users guide, *GFDL Ocean Group Tech. Rep. 2*, Geophys. Fluid Dyn. Lab., Princeton, N. J., 1993.

Packard, T. T., M. Denis, and P. Garfield, Deep-ocean metabolic CO_2 production: Calculations from ETS activity, *Deep Sea Res., Part A*, *35*, 371-382, 1988.

Peng, T. H., T. Takahashi, and W. S. Broecker, Seasonal variability of carbon dioxide, nutrients and oxygen in the northern Atlantic surface water: Observations and a model, *Tellus, Ser. B*, *39*, 439-458, 1987.

Quay, P. D., B. Tilbrook, and C. S. Wong, Oceanic uptake of fossil fuel CO_2: Carbon-13 evidence, *Science*, *256*, 74-79, 1992.

Quinby-Hunt, M. S., and K. K. Turekian, Distribution of elements in sea water, *Eos Trans. AGU*, *64*, 130-132, 1983.

Sarmiento, J. L., Oceanic uptake of anthropogenic CO_2: The major uncertainties, *Global Biogeochem. Cycles*, *5*, 309-313, 1991.

Sarmiento, J. L., and J. C. Orr, Three-dimensional simulations of the impact of Southern Ocean nutrient depletion on atmospheric CO_2 and ocean chemistry, *Limnol. Oceanogr.*, *36*, 1928-1950, 1991.

Sarmiento, J. L., and E. T. Sundquist, Revised budget for the oceanic uptake of anthropogenic carbon dioxide, *Nature*, *356*, 589-593, 1992.

Sarmiento, J. L., J. R. Toggweiler, and R. Najjar, Ocean carbon cycle dynamics and atmospheric pCO_2, *Philos. Trans. R. Soc. London, Ser. B*, *325*, 3-21, 1988.

Sarmiento, J. L., J. C. Orr, and U. Siegenthaler, A perturbation simulation of CO_2 uptake in an ocean general circulation model, *J. Geophys. Res.*, *97*, 3621-3646, 1992.

Sarmiento, J. L., R. D. Slater, M. J. R. Fasham, H. W. Ducklow, J. R. Toggweiler, and G. T. Evans, A seasonal three-dimensional ecosystem model of nitrogen cycling in the North Atlantic euphotic zone, *Global Biogeochem. Cycles*, *7*, 417-450, 1993.

Sarmiento, J. L., R. Murnane, and C. L. Quéré, Air-sea CO_2 transfer and the carbon budget of the North Atlantic, *Philos. Trans. R. Soc. London, Ser. B*, *348*, 211-219, 1995.

Schimel, D., I. G. Enting, M. Heimann, T. M. L. Wigley, D. Raynaud, D. Alves, and U. Siegenthaler, CO_2 and the Carbon Cycle, in *Climate Change 1994*, edited by J. T. Houghton et al., pp. 35-71, Cambridge Univ. Press, New York, 1995.

Schmitz, W. J., and M. S. McCartney, On the North Atlantic circulation, *Rev. Geophys.*, *31*, 29-49, 1993.

Semtner, A. J., and R. M. Chervin, Ocean general circulation from a global eddy-resolving model, *J. Geophys. Res.*, *97*, 5493-5550, 1992.

Siegenthaler, U., and F. Joos, Use of simple model for studying oceanic tracer distributions and the global carbon cycle, *Tellus, Ser. B*, *44*, 186-207, 1992.

Siegenthaler, U., and J. L. Sarmiento, Atmospheric carbon dioxide and the ocean, *Nature*, *365*, 119-125, 1993.

Sjoberg, S., A. Nordin, and N. Ingri, Equilibrium and structural studies of silicon(IV) and aluminium(III) in aqueous solution II: Formation constants for the monosilicate ions $SiO(OH)^-_3$ and $SiO_2(OH)^{2-}_2$: A precision study at 25°C in a simplified seawater medium, *Mar. Chem.*, *10*, 521-532, 1981.

Takahashi, T., T. T. Takahashi, and S. C. Sutherland, An assessment of the role of the North Atlantic as a CO_2 sink, *Philos. Trans. R. Soc. London, Ser. B*, *348*, 143-151, 1995.

Takahashi, T., R. A. Feely, R. F. Weiss, R. H. Wanninkhof, D. W. Chipman, S. C. Sutherland, and T. T. Takahashi, Global air-sea flux of CO_2: an estimate based on measurements of sea-air pCO_2 difference, *Proc. Natl. Acad. Sci. U. S. A.*, *94*, 8292-8299, 1997.

Talley, L. D., Meridional heat transport in the Pacific Ocean, *J. Phys. Oceanogr.*, *14*, 231-241, 1984.

Tans, P. P., I. Y. Fung, and T. Takahashi, Observational constraints on the global atmospheric CO_2 budget, *Science*, *247*, 1431-1438, 1990.

Toggweiler, J. R., and B. Samuels, Is the magnitude of the deep outflow from the Atlantic Ocean actually governed by Southern Hemisphere winds?, in *The Global Carbon Cycle*, edited by M. Heimann, pp. 303-331, Springer-Verlag, New York, 1993a.

Toggweiler, J. R., and B. Samuels, New radiocarbon constraints on the upwelling abyssal water to the ocean's surface, in *The Global Carbon Cycle*, edited by M. Heimann, pp. 333-366, Springer-Verlag, New York, 1993b.

Toggweiler, J. R., K. Dixon, and K. Bryan, Simulation of radiocarbon in a coarse-resolution world ocean model, 1, Steady state prebomb distributions, *J. Geophys. Res.*, *94*, 8217-8242, 1989.

Uppström, L. R., The boron/chlorinity ratio of deep-sea water from the Pacific Ocean, *Deep Sea Res. Oceanogr. Abstr.*, *21*, 161-162, 1974.

Volk, T., and M. I. Hoffert, Ocean carbon pumps: Analysis of relative strengths and efficiencies in ocean-driven atmospheric CO_2 changes, in *The Carbon Cycle and Atmospheric CO_2: Natural Variations Archean to Present, Geophys. Monogr. Ser.*, vol. 32, edited by E. T. Sundquist and W. S. Broecker, pp. 99-110, AGU, Washington, D. C., 1985.

Volk, T., and Z. Liu, Controls of CO_2 sources and sinks in the Earth scale surface ocean: Temperature and nutrients, *Global Biogeochem. Cycles*, *2*, 73-89, 1988.

Wanninkhof, R., Relationship between wind speed and gas exchange over the ocean, *J. Geophys. Res.*, *97*, 7373-7383, 1992.

Weiss, R. F., Carbon dioxide in water and seawater: The solubility of a non-ideal gas, *Mar. Chem.*, *2*, 203-215, 1974.

Winguth, A. M. E., M. Heimann, K. D. Kurz, E. Maier-Reimer, U. Mikolajewicz, and J. Segschneider, El Nino-Southern Oscillation related fluctuations of the marine carbon cycle, *Global Biogeochem. Cycles*, *8*, 39-63, 1994.

Yamanaka, Y., and E. Tajika, The role of the vertical fluxes of particulate organic matter and calcite in the oceanic carbon cycle: Studies using an ocean biogeochemical general circulation model, *Global Biogeochem. Cycles*, *10*, 361-382, 1996.

Yamanaka, Y., and E. Tajika, Role of dissolved organic matter in the marine biogeochemical cycle: Studies using an ocean biogeochemical general circulation model, *Global Biogeochem. Cycles*, *11*, 599-612, 1997.

C. Le Quéré, Laboratoire des Sciences du Climat et de l'Environement, L'Orme des Merisiers, Bat. 701, 91191 Gif-sur-Yvette, France. (lequere@lsce.saclay.cea.fr)

R. J. Murnane, Risk Prediction Initiative, Bermuda Biological Station for Research, Ferry Reach, St. George's GE01, Bermuda. (rmurnane@bbsr.edu)

J. L. Sarmiento, Program in Atmospheric and Oceanic Sciences, Department of Geosciences, Princeton University, Princeton, NJ 08544. (jls@splash.princeton.edu)

(Received April 4, 1997; revised June 17, 1998;
accepted July 10, 1998.)